Electronic Supplementary Information

Multi PCET in Symmetrically Substituted Benzimidazoles

Emmanuel Odella,[§] Maxim Secor,[†] Mackenna Elliot,[§] Thomas L. Groy,[§] Thomas A. Moore,[§] Sharon Hammes-Schiffer,*[,†] and Ana L. Moore*[,§]

§ School of Molecular Sciences, Arizona State University, Tempe, Arizona 85287-1604, United States.

† Department of Chemistry, Yale University, New Haven, Connecticut 06520-8107, United States.

*corresponding authors: sharon.hammes-schiffer@yale.edu and amoore@asu.edu.

Table of Contents

1. Experimental Results

1.1. Materials and Methods

NMR characterization was carried out at 25 °C using a 500 MHz Bruker spectrometer, employing standard pulse techniques. Samples were dissolved in $CDCl_3$, CD_2Cl_2, $(CD_3)_2CO$ or $(CD_3)_2SO$ and chemical shifts were measured relative to internal TMS (0.05% v/v). Mass spectra were obtained with a Voyager DE STR matrix assisted laser desorption/ionization time-of-flight (MALDI-TOF) mass spectrometer in positive or negative ion mode and *trans*, *trans*-1,4-diphenyl-1,3-butadiene was used as the matrix. All chemicals were purchased from Aldrich, Acros or Alfa Aesar. Solvents were obtained from VWR. Thin layer chromatography (TLC) was performed with silica gel coated glass plates from Merck Millipore. Column chromatography was carried out using Silicycle silica gel 60 having 230-400 mesh.

Cyclic Voltammetry: Cyclic voltammetry measurements were performed with a CH Instruments 760C potentiostat using a glassy carbon (3 mm diameter) working electrode, a Pt wire counter electrode, and a Ag wire pseudoreference electrode in a conventional three-electrode cell. All cyclic voltammograms (CVs) were collected in anhydrous dichloromethane, previously distilled and kept over molecular sieves and K_2CO_3, containing the compound of interest at a concentration of 1 mM. Tetrabutylammonium hexafluorophosphate ($TBAPF_6$, 0.1 M in dichloromethane) was used as the supporting electrolyte. All measurements were conducted at room temperature under an argon atmosphere and the scan rate was 100 mV s^{-1}. The glassy carbon working electrode was polished between measurements with an aluminum slurry on a microcloth polishing pad, followed by solvent rinses and drying under a stream of nitrogen. The potential of the pseudoreference electrode was determined using the ferrocenium/ferrocene redox couple as an internal standard and adjusting to the saturated calomel electrode (SCE) scale (with $E_{1/2}$ taken to be 0.46 V *vs* SCE in dichloromethane).[1]

FTIR and Infrared Spectroelectrochemistry (IRSEC): FTIR measurements were performed using a Bruker Vertex 70 spectrometer in absorption mode under a dry nitrogen purge with a 2 cm^{-1} resolution, GloBar MIR source, broadband KBr beamsplitter, and liquid nitrogen cooled MCT detector. Spectra were collected in anhydrous dichloromethane at a concentration of 15 mM of **3**, using 0.1 M $TBAPF_6$ as supporting electrolyte. IRSEC measurements were conducted using a Biologic potentiostat connected to an optically transparent thin-layer electrochemical cell

(Spectroelectrochemistry Reading RT OTTLE cell) equipped with CaF_2 optical windows (pathlength 0.2 mm). The cell has a Pt mesh counter electrode, a Ag wire pseudoreference electrode, and a Pt mesh working electrode that was positioned in the light path of the IR spectrophotometer. A complete and detailed description of the spectroelectrochemical technique is described elsewhere.[2]

1.2. Synthesis and Structural Characterization

The synthetic approach for the preparation of **3** is shown in Scheme S1.

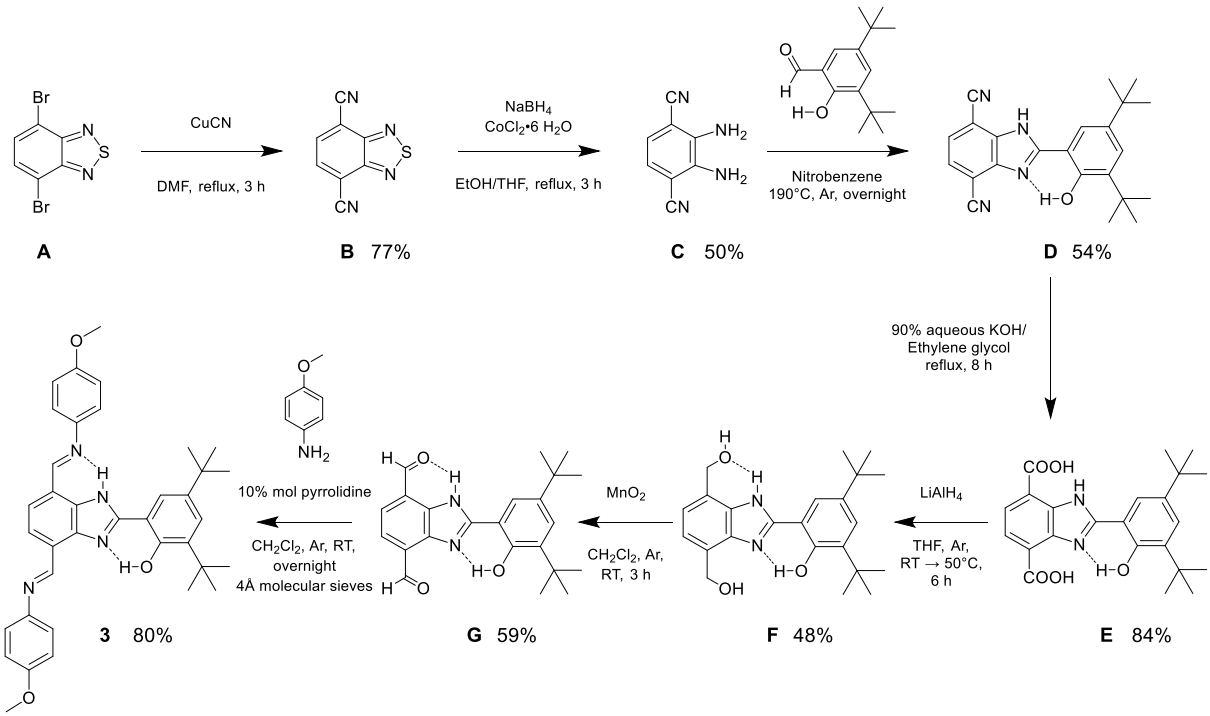

Scheme S1. Synthetic strategy detailing reactions conditions, yields, and intermediate molecules for preparation of **3**.

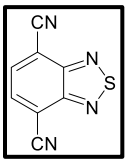

4,7-Di-cyano-2,1,3-benzothiadiazole (B)

A similar method has been reported.[3] A portion of copper cyanide (2.20 g, 24.6 mmol) was dissolved in dry DMF (45 mL), and 4,7-dibromo-2,1,3-benzothiadiazole (**A**, 2.26 g, 7.7 mmol) was then added to the solution and stirred under argon for 15 minutes. The mixture was refluxed for 3 hours under argon. A separate solution of $FeCl_3$•$6H_2O$ (10.2 g, 37.7 mmol) in 18.5 mL of HCl 15% v/v was prepared. Once the refluxed mixture cooled to room temperature, the resulting $FeCl_3$•$6H_2O$ solution was added to the cooled reaction mixture and stirred at 20 °C for 0.5 hours. The crude product was extracted with dichloromethane (3 × 100 mL), and the combined organic layers were washed first with a 6 M HCl solution (3 × 100 mL), water (3 × 100 mL), and finally brine (3 × 100 mL). The organic layer was then dried over Na_2SO_4, and the solvent was removed under reduced pressure. The residue was purified by flash column chromatography on silica gel using hexanes/ethyl acetate (40:60) to afford 1.10 g of **B** (77 % yield). ^{1}H NMR (500 MHz, $(CD_3)_2CO$) δ 8.51 (s, 2H, ArH). NMR characterization is in line with previously reported spectrum.[3] MALDI-TOF-MS *m/z.* calcd. for $C_8H_2N_4S$: 186.000, experimental (M^+): 186.004.

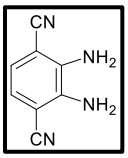

2,3-Diaminoterephthalonitrile (C)

A similar method has been reported.[3] A portion of **B** (1.02 g, 5.5 mmol) was suspended in a solvent mixture of ethanol (45.5 mL) and freshly distilled tetrahydrofuran (4.5 mL). $CoCl_2$•$6H_2O$ (119 mg, 0.5 mmol) was added to the solution and it was stirred under argon for 15 minutes. A portion of $NaBH_4$ (1.04 g, 27.5 mmol) was added, and the solution was refluxed for 1.5 hours. A second portion of $NaBH_4$ (416 mg, 11.0 mmol) was then added and refluxed for an extra 0.5 hours. The solution was filtered with a Celite pad and the solvents were removed under reduced pressure. The dried, crude product was dissolved in water (200 mL) and extracted using 10% methanol in dichloromethane (3 × 100 mL). The organic extracts were combined, dried over Na_2SO_4, and the

solvents were removed under reduced pressure. The residue was purified by flash column chromatography on silica gel using hexanes/ethyl acetate mixture (50:50) to afford 430 mg of **C** (50 % yield). The solid was immediately used in the next step to avoid decomposition. ^{1}H NMR (500 MHz, $(CD_3)_2SO$) δ 6.06 (s, 4H, NH_2), 6.71 (s, 2H, ArH). NMR characterization is in line with previously reported spectrum.[4] MALDI-TOF-MS *m/z.* calcd. for $C_8H_5N_4$: 157.051, experimental $(M-H)^+$: 157.055.

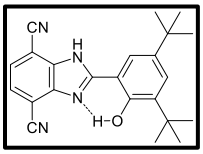

4,7-Di-cyano-2-(3',5'-di-*tert*-butyl-2'-hydroxyphenyl)benzimidazole (D)

Synthesis of **D** was achieved following a well-known procedure.[2] A portion of 3,5-di-*tert*-butyl-2-hydroxybenzaldehyde (562 mg, 2.4 mmol) in nitrobenzene (9 mL) was added drop-wise to a solution of **C** (380 mg, 2.4 mmol) in nitrobenzene (9 mL) under argon atmosphere. The mixture was stirred for 30 minutes and then heated overnight at 190 °C. The solvent was removed under reduced pressure and the residue was purified by column chromatography on silica gel using dichloromethane/hexanes mixtures (80:20 → 90:10) to give 483 mg of **D** (54 % yield). ^{1}H NMR (500 MHz, $(CD_3)_2CO$) δ 1.35 (s, 9H, $C(CH_3)_3$), 1.52 (s, 9H, $C(CH_3)_3$), 7.61 (d, J = 2.3 Hz, 1H, ArH), 7.89 (s, 2H, ArH) 8.05 (d, J = 2.3 Hz, 1H, ArH), 12.99 (br, 1H, NH), 13.40 (br, 1H, OH). ^{13}C NMR (126 MHz, $(CD_3)_2CO$) δ 29.9 (overlap with solvent signal), 31.7, 35.2, 36.0, 111.2, 116.0, 122.2, 127.7, 128.2, 129.3, 138.4, 142.3, 157.2, 157.5, 158.2. MALDI-TOF-MS *m/z.* calcd. for $C_{23}H_{25}N_4O$: 373.202, experimental $(M-H)^+$: 373.201.

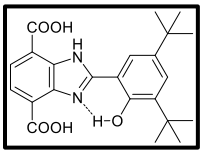

4,7-Dicarboxylic acid-2-(3',5'-di-*tert*-butyl-2'-hydroxyphenyl)benzimidazole (E)

Compound **D** (470 mg, 1.3 mmol) was added to a 90% KOH aqueous solution (13 mL) and ethylene glycol (19 mL), and the mixture heated under reflux for 8 hours. The reaction mixture was cooled down, diluted with water (100 mL), and extracted with ethyl acetate (3 × 80 mL). The

resulting aqueous layer was adjusted to pH = 6 with 1M HCl solution, and the resulting precipitate was collected by filtration and dried under reduced pressure. No further purification was performed and the solid was used in the next reaction (450 mg, 84 % yield). ^{1}H NMR (500 MHz, $(CD_3)_2SO$) δ 1.37 (s, 9H, $C(CH_3)_3$), 1.45 (s, 9H, $C(CH_3)_3$), 7.40 (d, *J* = 2.2 Hz, 1H, ArH), 7.91 (s, 2H, ArH), 8.29 (d, *J* = 2.4 Hz, 1H, ArH), 12.54-14.00 (br, 3H, NH and COOH), 14.52 (s, 1H, OH). ^{13}C NMR (126 MHz, $(CD_3)_2SO$) δ 29.4, 31.5, 34.4, 34.9, 110.8, 122.6, 124.2, 126.5, 135.9, 139.8, 155.6, 156.1, 166.2. MALDI-TOF-MS *m/z*. calcd. for $C_{23}H_{27}N_2O_5$: 411.191, experimental $(M+H)^+$: 411.192.

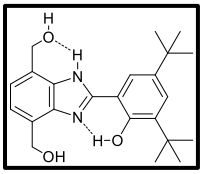

4,7-Di-hydroxymethyl-2-(3',5'-di-*tert*-butyl-2'-hydroxyphenyl)benzimidazole (F)

A portion of **E** (402 mg, 1.0 mmol) was dissolved in freshly distilled THF (10 mL) and stirred under argon for 15 minutes. At room temperature, an excess of lithium aluminum hydride was added to the mixture and heated at 50 °C. The reaction was followed by TLC until completion (approximately 6 hours). The solution was cooled down, and water was added drop-wise to deactivate the excess $LiAlH_4$. The reaction mixture was then filtered through a pad of Celite and washed with 15% methanol in dichloromethane and dried under reduced pressure. The residue was then dissolved in water (100 mL) and extracted using 15% methanol in dichloromethane (3 × 100 mL), controlling the pH of the aqueous phase at around 8. The organic extracts were combined, dried over Na_2SO_4, and the solvent was removed under reduced pressure. The residue was purified by flash column chromatography on silica gel using 3% methanol in dichloromethane to afford 181 mg of **F**. (48 % yield). ^{1}H NMR (500 MHz, $(CD_3)_2CO$) δ 1.34 (s, 9H, $C(CH_3)_3$), 1.51 (s, 9H, $C(CH_3)_3$), 4.23 (br, 1H, CH_2OH), 4.29 (br, 1H, CH_2OH), 4.88 (s, 2H, CH_2OH), 5.11 (s, 2H, CH_2OH), 7.25 (d, *J* = 7.5 Hz, 1H, ArH), 7.35 (d, *J* = 7.5 Hz, 1H, ArH), 7.47 (d, *J* = 2.3 Hz, 1H, ArH), 7.98 (d, *J* = 2.3 Hz, 1H, ArH), 11.97 (br, 1H, NH), 13.88 (br, 1H, OH). ^{13}C NMR (126 MHz, $(CD_3)_2CO$) δ 29.9, 31.9, 35.1, 35.9, 60.7, 62.0, 112.8, 121.0, 121.3, 122.8, 125.4, 126.9, 131.9, 131.9, 137.6, 140.0, 141.3, 153.5, 156.8. MALDI-TOF-MS *m/z*. calcd. for $C_{23}H_{30}N_2O_3$: 382.226, experimental $(M)^+$: 382.229.

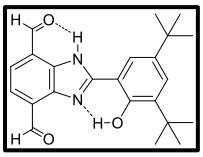

4,7-Di-formyl-2-(3',5'-di-*tert*-butyl-2'-hydroxyphenyl)benzimidazole (G)

Compound **F** (176 mg, 0.5 mmol) was dissolved in dichloromethane (50 mL) and stirred under argon for 15 minutes. Activated MnO_2 was added carefully at room temperature, and the reaction was followed by TLC. After completion (approximately 3 hours), the mixture was filtered through a Celite pad and the residue washed with 5% methanol in dichloromethane, and the solvent was removed under reduced pressure. The solid was purified by flash column chromatography on silica gel using dichloromethane as the eluent to afford 103 mg of **G** (59 % yield). ^{1}H NMR (500 MHz, $CDCl_3$) δ 1.41 (s, 9H, $C(CH_3)_3$), 1.52 (s, 9H, $C(CH_3)_3$), 7.52 (d, *J* = 2.3 Hz, 1H, ArH), 7.55 (d, *J* = 2.3 Hz, 1H, ArH), 7.85 (d, *J* = 7.8 Hz, 1H, ArH), 7.99 (d, *J* = 7.8 Hz, 1H, ArH), 10.23 (s, 1H, CHO), 10.96 (s, 1H, CHO), 11.04 (s, 1H, NH), 12.96 (s, 1H, OH). ^{13}C NMR (126 MHz, $CDCl_3$) δ 29.5, 31.6, 34.5, 35.4, 110.0, 119.3, 121.3, 123.3, 127.4, 128.5, 128.7, 132.8, 138.3, 141.3, 143.7, 156.6, 156.7, 189.2, 192.7. MALDI-TOF-MS *m/z.* calcd. for $C_{23}H_{27}N_2O_3$: 379.202, experimental $(M+H)^+$: 379.202.

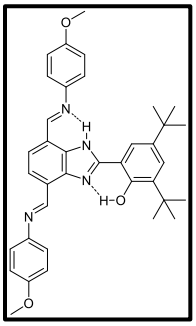

4,7-Di-(4-methoxyphenyliminomethyl)-2-(3',5'-di-*tert*-butyl-2'-hydroxyphenyl)benzimidazole (3)

Compound **G** (50 mg, 0.13 mmol) was dissolved in 15 mL of dry dichloromethane containing 4Å molecular sieves. The mixture was stirred under an argon atmosphere and *p*-anisidine (32 mg, 0.26 mmol) was added. Then 1.00 µL of pyrrolidine (0.013 mmol) was added. After 24 hours, the reaction mixture was filtered and the molecular sieves washed several times with dry dichloromethane. The solvent was removed under reduced pressure, and the crude product

was recrystallized from dichloromethane/hexanes mixture to give 62 mg of **3** (80 % yield). Single crystals of **3** were grown by the vapor diffusion technique using dichloromethane and hexanes as solvents (see Crystal Structure and X-Ray Data for Compound **3**). ^{1}H NMR (500 MHz, $CDCl_3$) δ 1.42 (s, 9H, $C(CH_3)_3$), 1.53 (s, 9H, $C(CH_3)_3$), 3.88 (s, 3H, OCH_3), 3.89 (s, 3H, OCH_3), 6.99 – 7.04 (m, 4H, ArH), 7.38 – 7.43 (m, 4H, ArH), 7.50 (d, *J* = 2.3 Hz, 1H, ArH), 7.54 (d, *J* = 2.3 Hz, 1H, ArH), 7.57 (d, *J* = 7.9 Hz, 1H, ArH), 8.19 (d, *J* = 7.9 Hz, 1H, ArH), 8.80 (s, 1H, CH═N), 9.39 (s, 1H, CH═N), 11.96 (br, 1H, NH), 13.13 (s, 1H, OH). ^{1}H NMR (500 MHz, CD_2Cl_2) δ 1.42 (s, 9H, $C(CH_3)_3$), 1.52 (s, 9H, $C(CH_3)_3$), 3.86 (s, 3H, OCH_3), 3.87 (s, 3H, OCH_3), 6.99 – 7.04 (m, 4H, ArH), 7.41 (d, *J* = 8.9 Hz, 2H, ArH), 7.45 (d, *J* = 8.7 Hz, 2H, ArH), 7.52 (d, *J* = 2.3 Hz, 1H, ArH), 7.59 (d, *J* = 2.3 Hz, 1H, ArH), 7.62 (d, *J* = 7.9 Hz, 1H, ArH), 8.16 (d, *J* = 7.9 Hz, 1H, ArH), 8.85 (s, 1H, CH═N), 9.37 (s, 1H, CH═N), 12.02 (br, 1H, NH), 13.20 (s, 1H, OH). ^{1}H NMR (500 MHz, $(CD_3)_2CO$) δ 1.43 (s, 9H, $C(CH_3)_3$), 1.53 (s, 9H, $C(CH_3)_3$), 3.87 (s, 3H, OCH_3), 3.88 (s, 3H, OCH_3), 7.05 – 7.10 (m, 4H, ArH), 7.45 – 7.50 (m, 2H, ArH), 7.55 – 7.60 (m, 3H, ArH), 7.82 (d, *J* = 7.9 Hz, 1H, ArH), 8.00 (d, *J* = 2.3 Hz, 1H, ArH), 8.19 (d, *J* = 7.9 Hz, 1H, ArH), 9.04 (s, 1H, CH═N), 9.43 (s, 1H, CH═N), 12.44 (br, 1H, NH), 13.49 (s, 1H, OH). ^{13}C NMR (126 MHz, $CDCl_3$) δ 29.5, 31.5, 34.3, 35.4, 55.5, 55.6, 110.9, 114.5, 114.8, 119.1, 119.8, 121.4, 122.4, 122.8, 126.1, 127.5, 128.1, 132.2, 137.9, 140.7, 142.2, 143.5, 145.0, 153.5, 154.0, 156.1, 156.8, 158.7, 159.1. MALDI-TOF-MS *m/z.* calcd. for $C_{37}H_{41}N_4O_3$: 589.317, experimental $(M+H)^+$: 589.319.

1.3. Nuclear Magnetic Resonance Data

Compound **B**

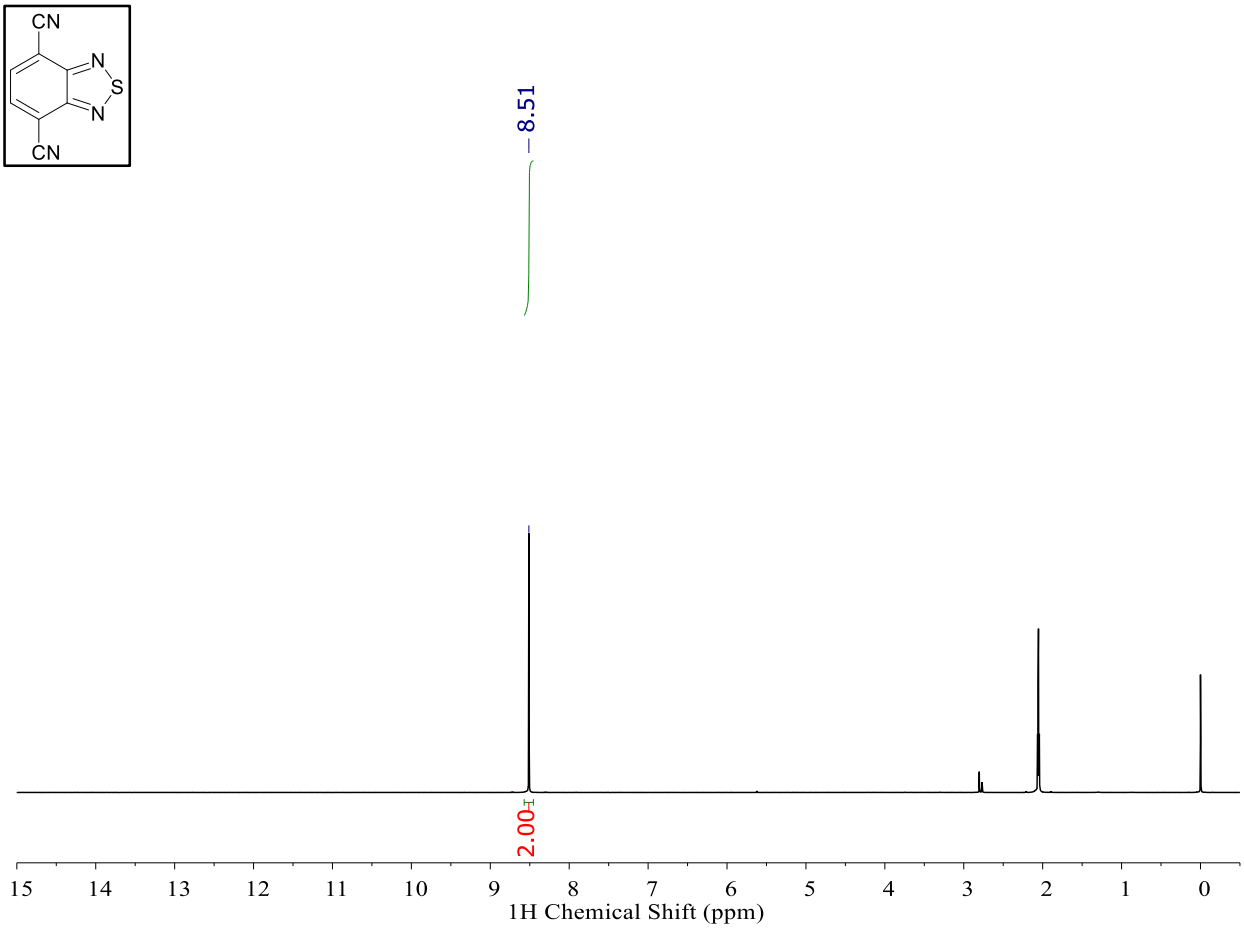

Figure S1. 500 MHz ^{1}H NMR spectrum of **B** in $(CD_3)_2CO$.

Compound **C**

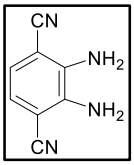

Figure S2. 500 MHz ^{1}H NMR spectrum of **C** in $(CD_3)_2SO$.

Compound **D**

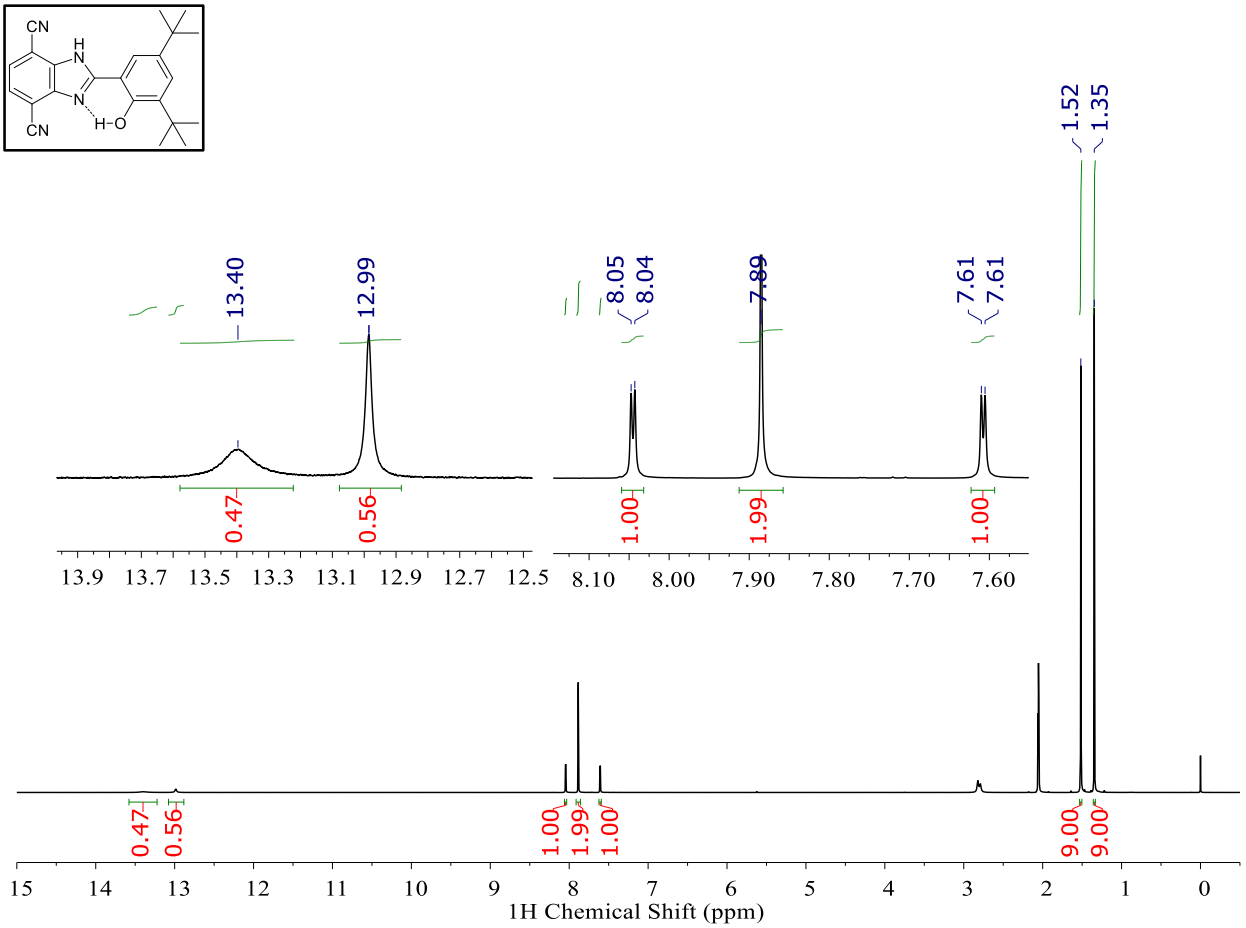

Figure S3. 500 MHz ^{1}H NMR spectrum of **D** in $(CD_3)_2CO$.

Compound **D**

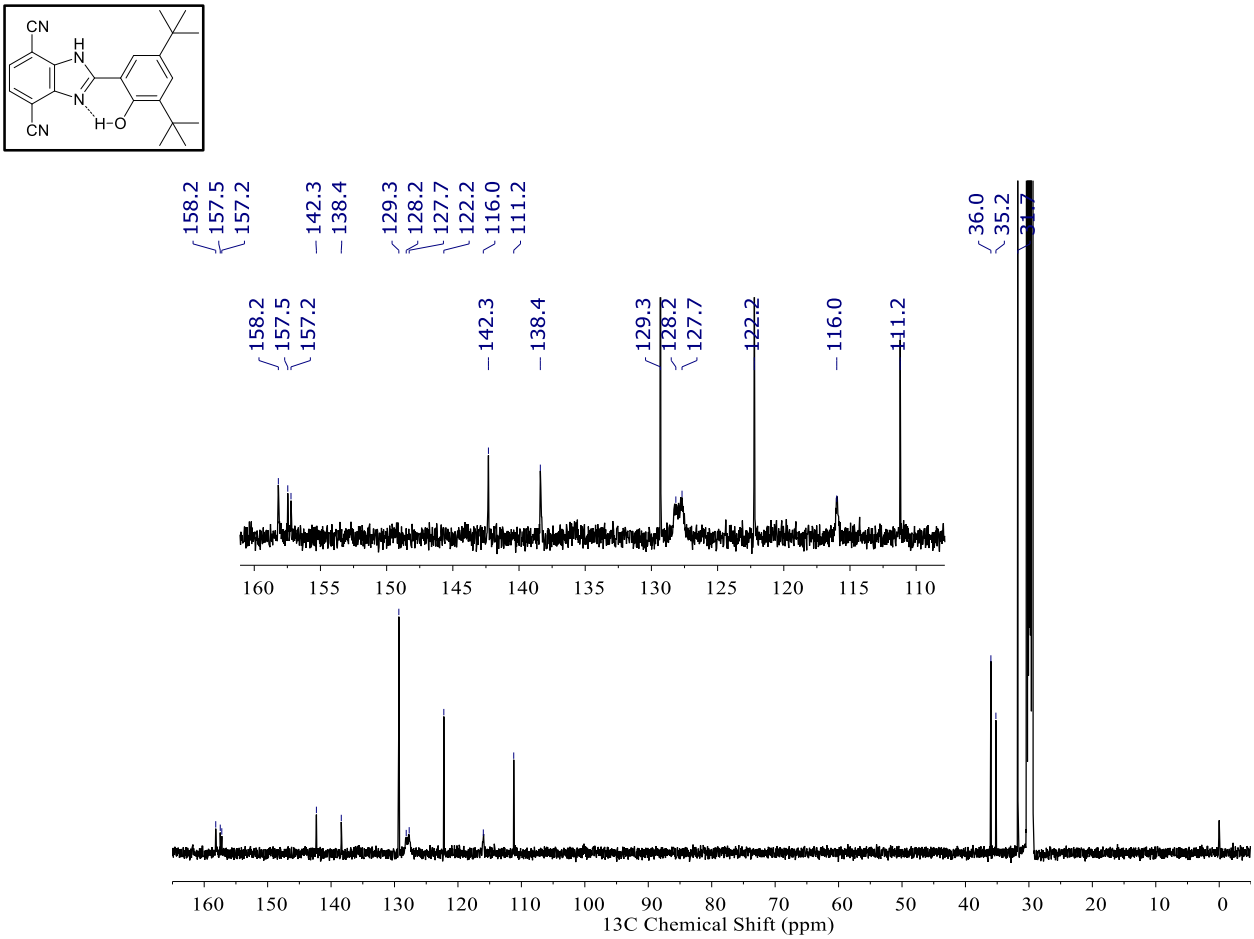

Figure S4. 126 MHz ^{13}C NMR spectrum of **D** in $(CD_3)_2CO$.

Compound **E**

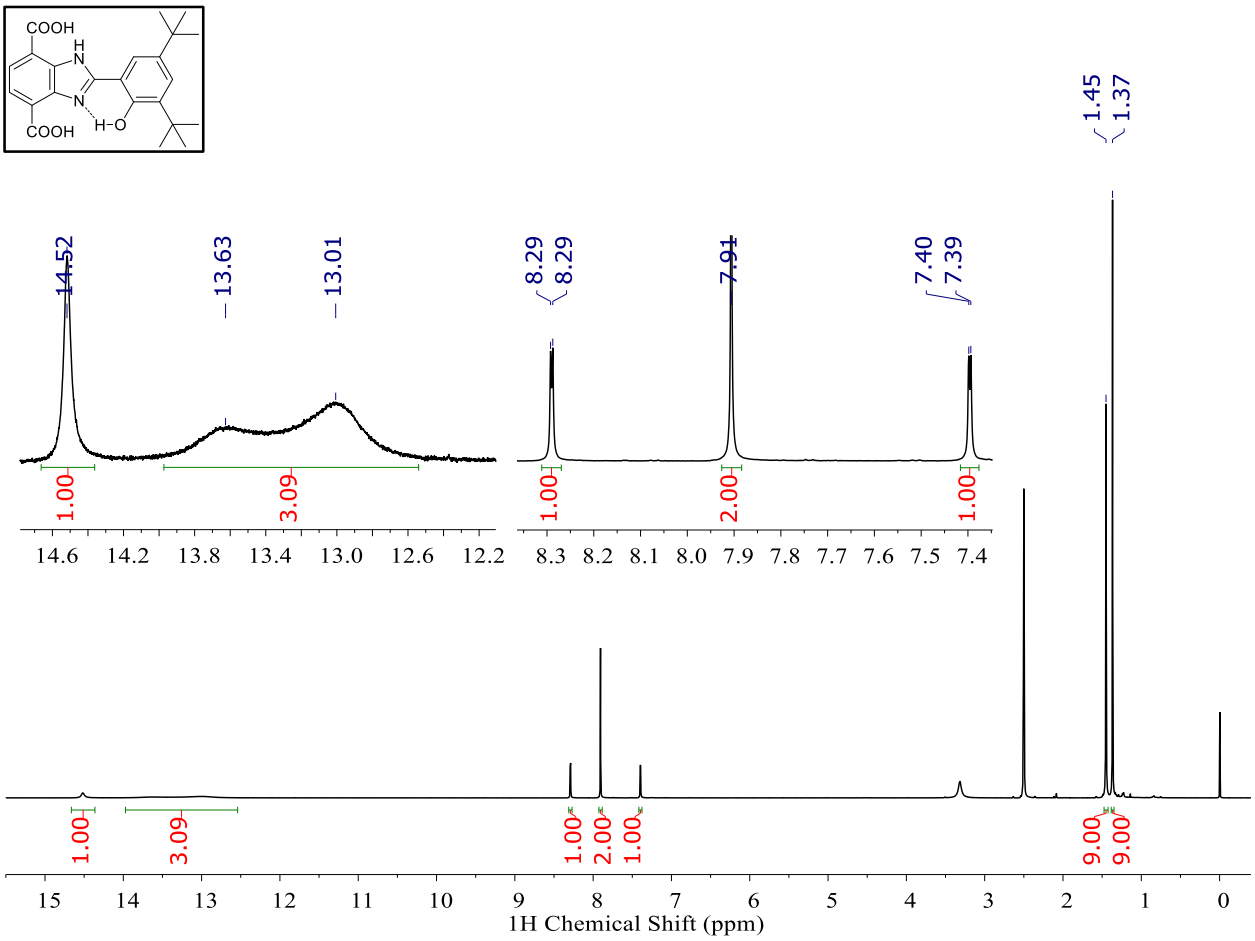

Figure S5. 500 MHz ^{1}H NMR spectrum of **E** in $(CD_3)_2SO$.

Compound **E**

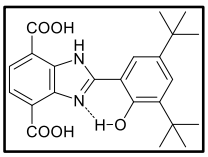

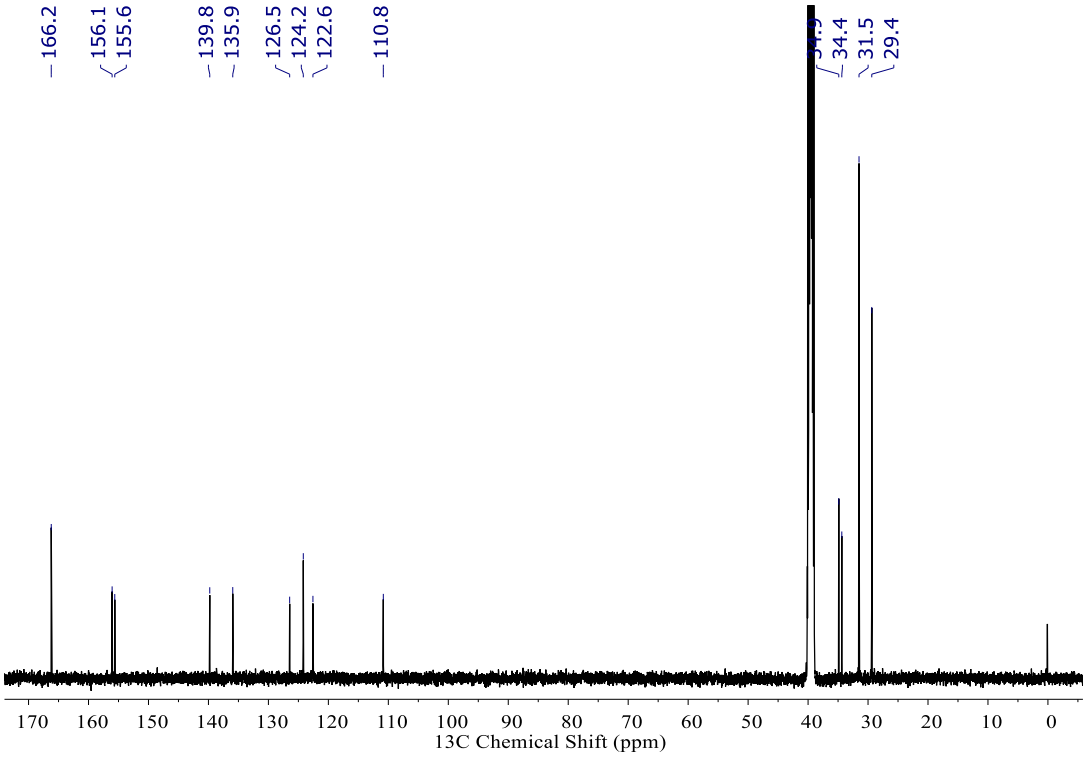

Figure S6. 126 MHz ^{13}C NMR spectrum of **E** in $(CD_3)_2SO$.

Compound **F**

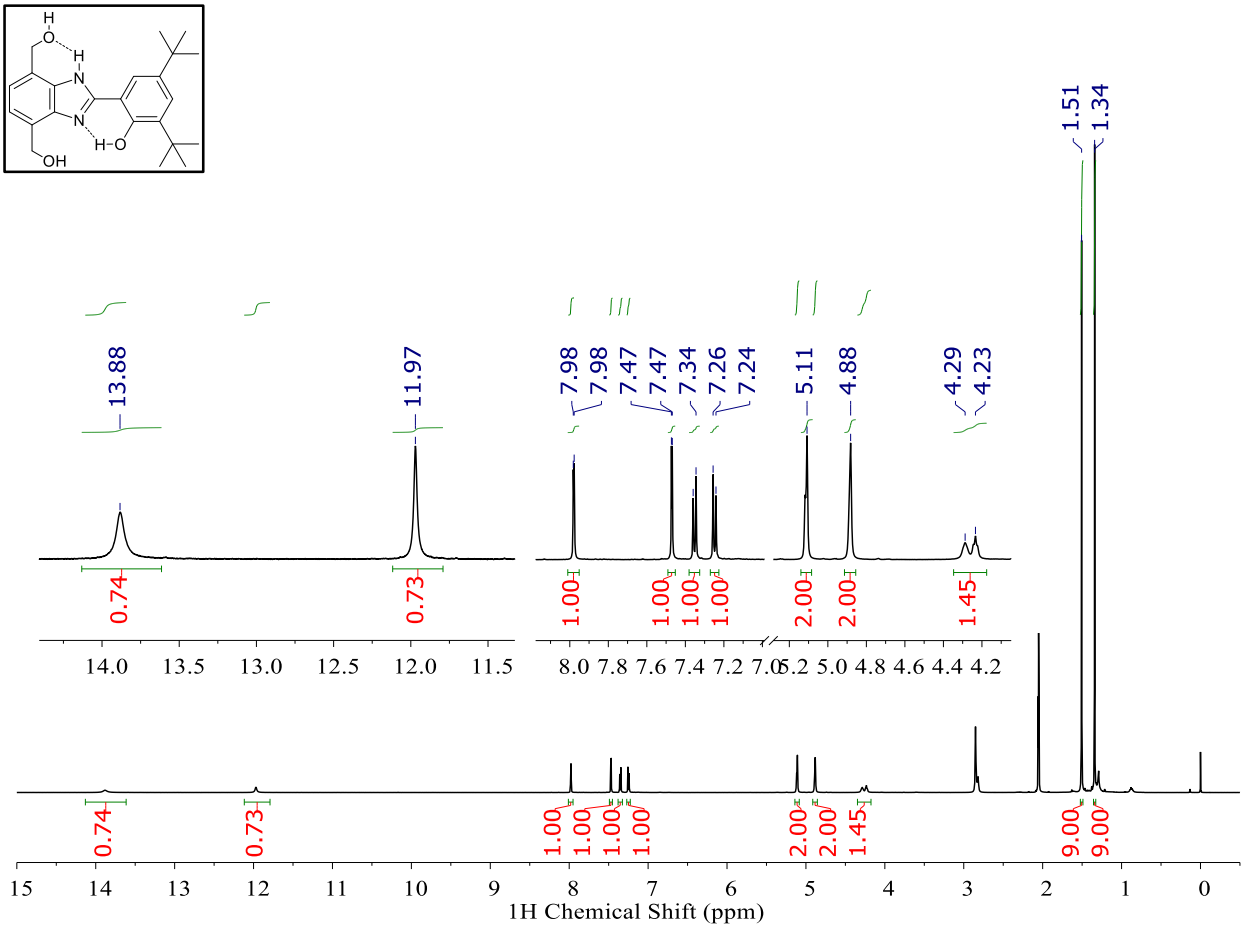

Figure S7. 500 MHz ^{1}H NMR spectrum of **F** in $(CD_3)_2CO$.

Compound **F**

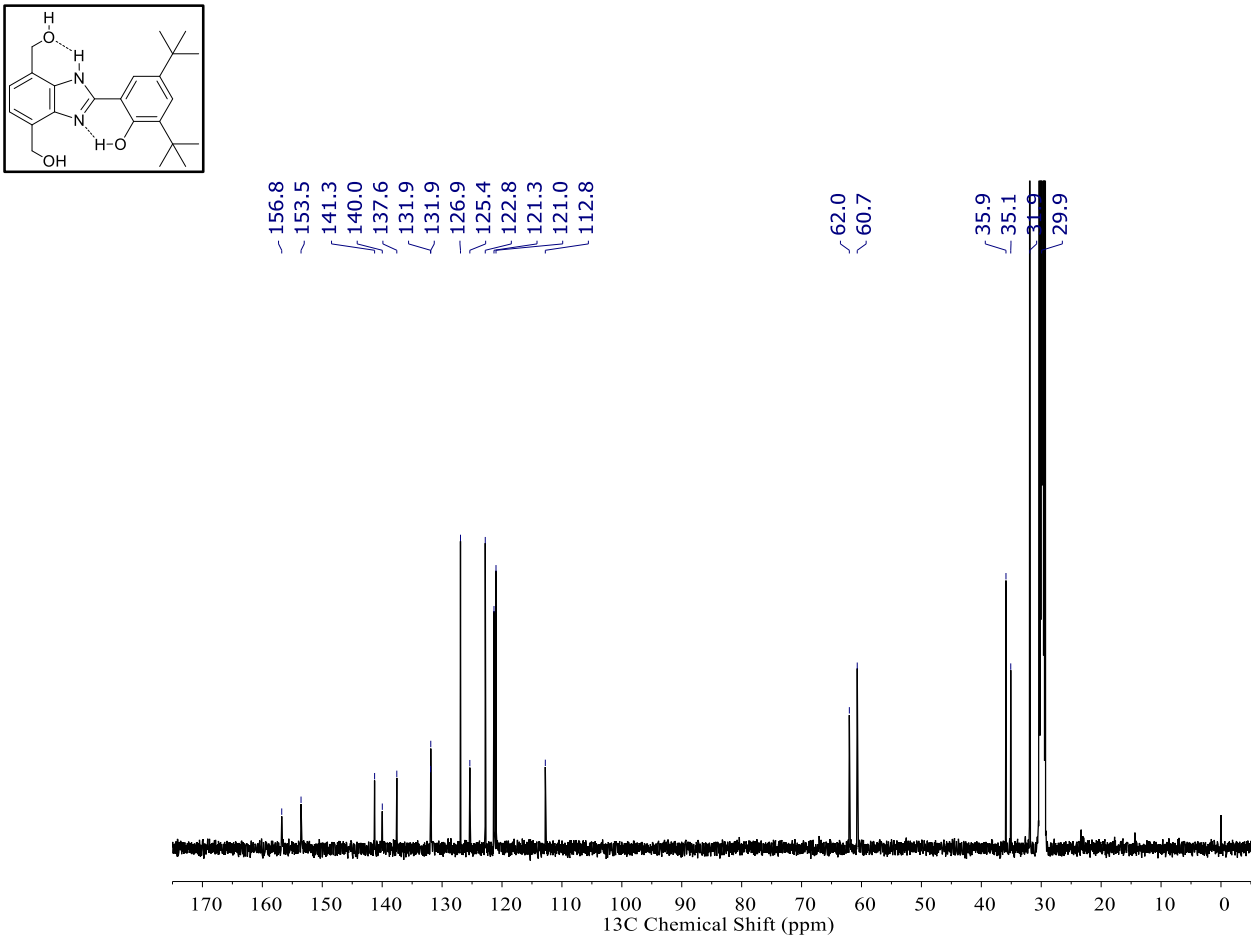

Figure S8. 126 MHz ^{13}C NMR spectrum of **F** in $(CD_3)_2CO$.

Compound **G**

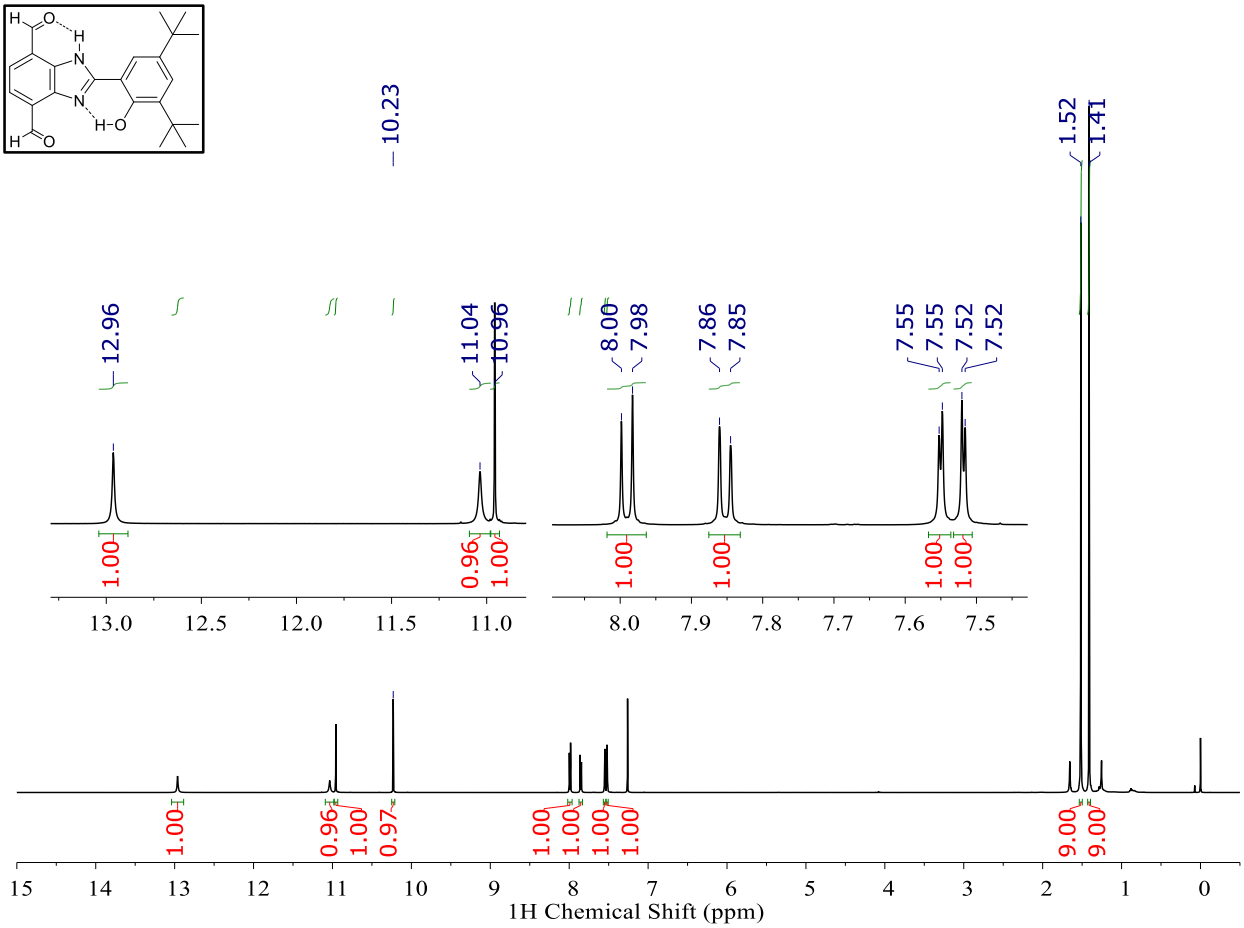

Figure S9. 500 MHz ^{1}H NMR spectrum of **G** in $CDCl_3$.

Compound **G**

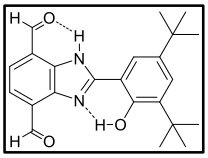

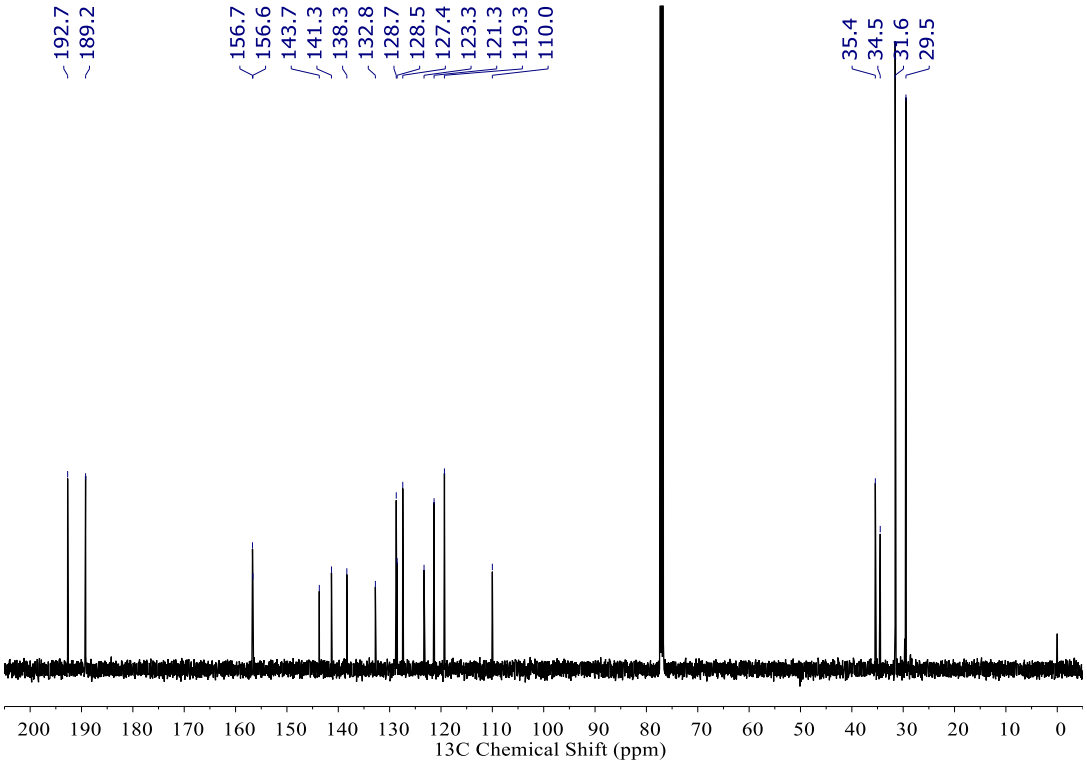

Figure S10. 126 MHz ^{13}C NMR spectrum of **G** in $CDCl_3$.

Compound **3**

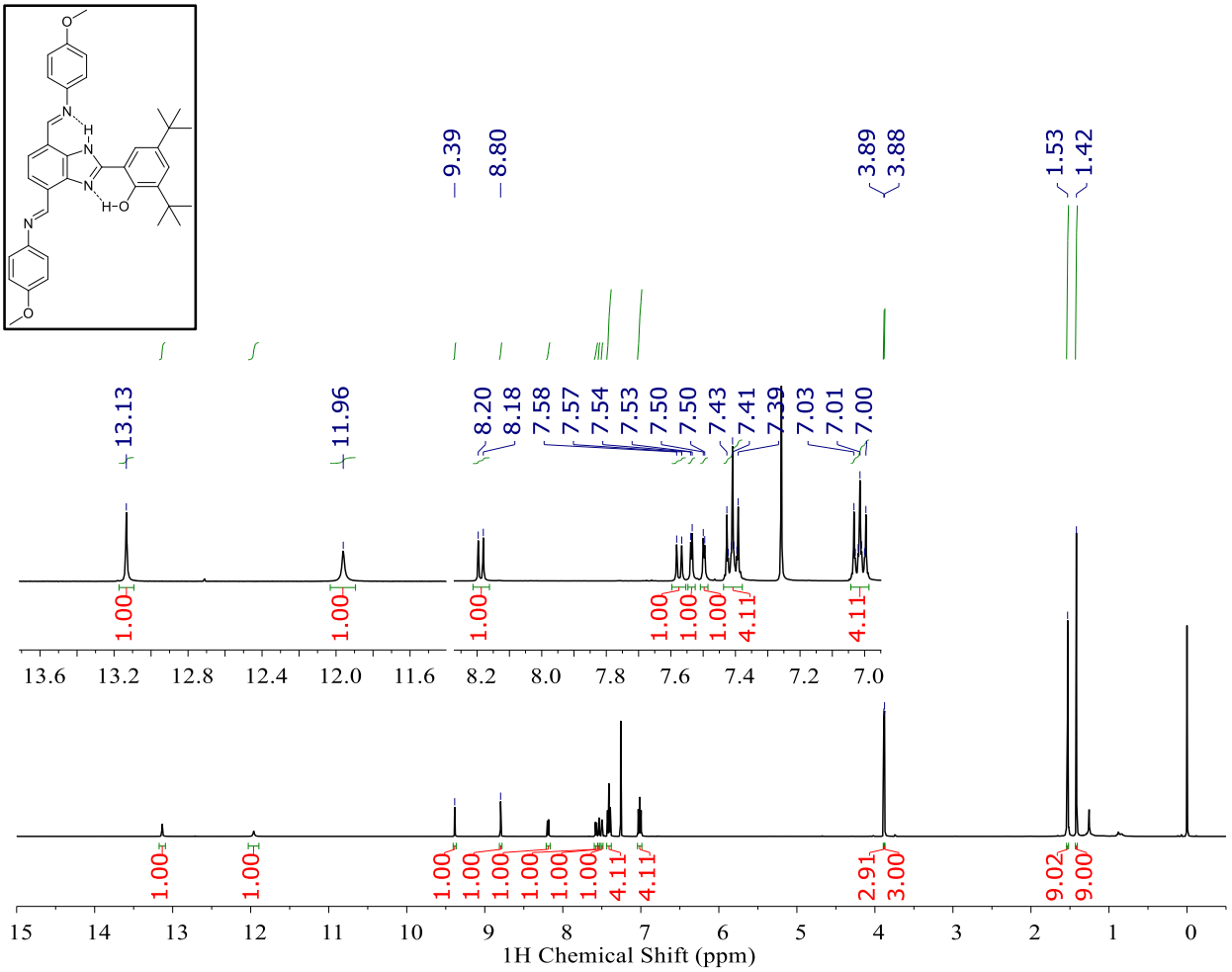

Figure S11. 500 MHz ^{1}H NMR spectrum of **3** in $CDCl_3$.

Compound **3**

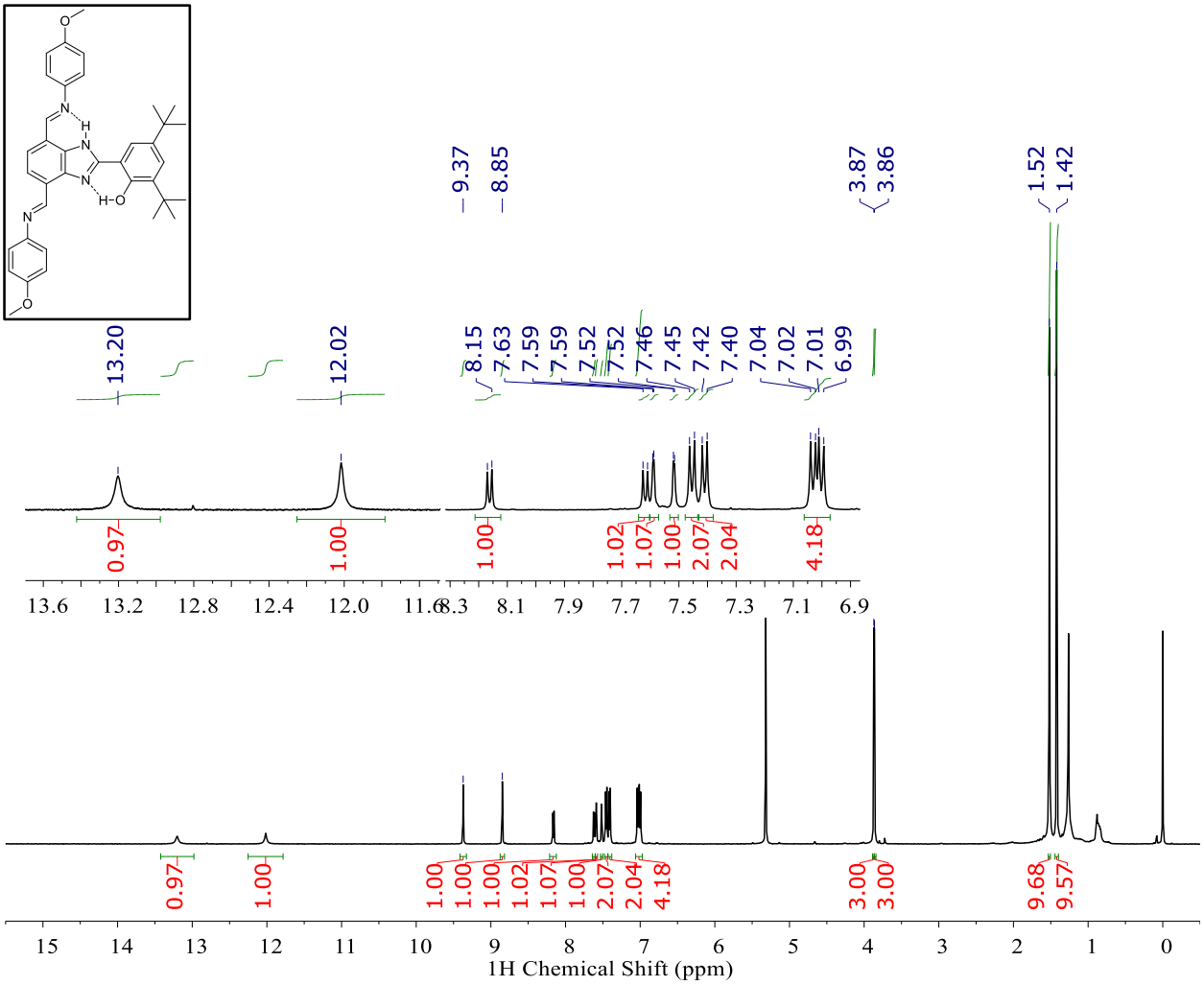

Figure S12. 500 MHz ^{1}H NMR spectrum of **3** in CD_2Cl_2.

Compound **3**

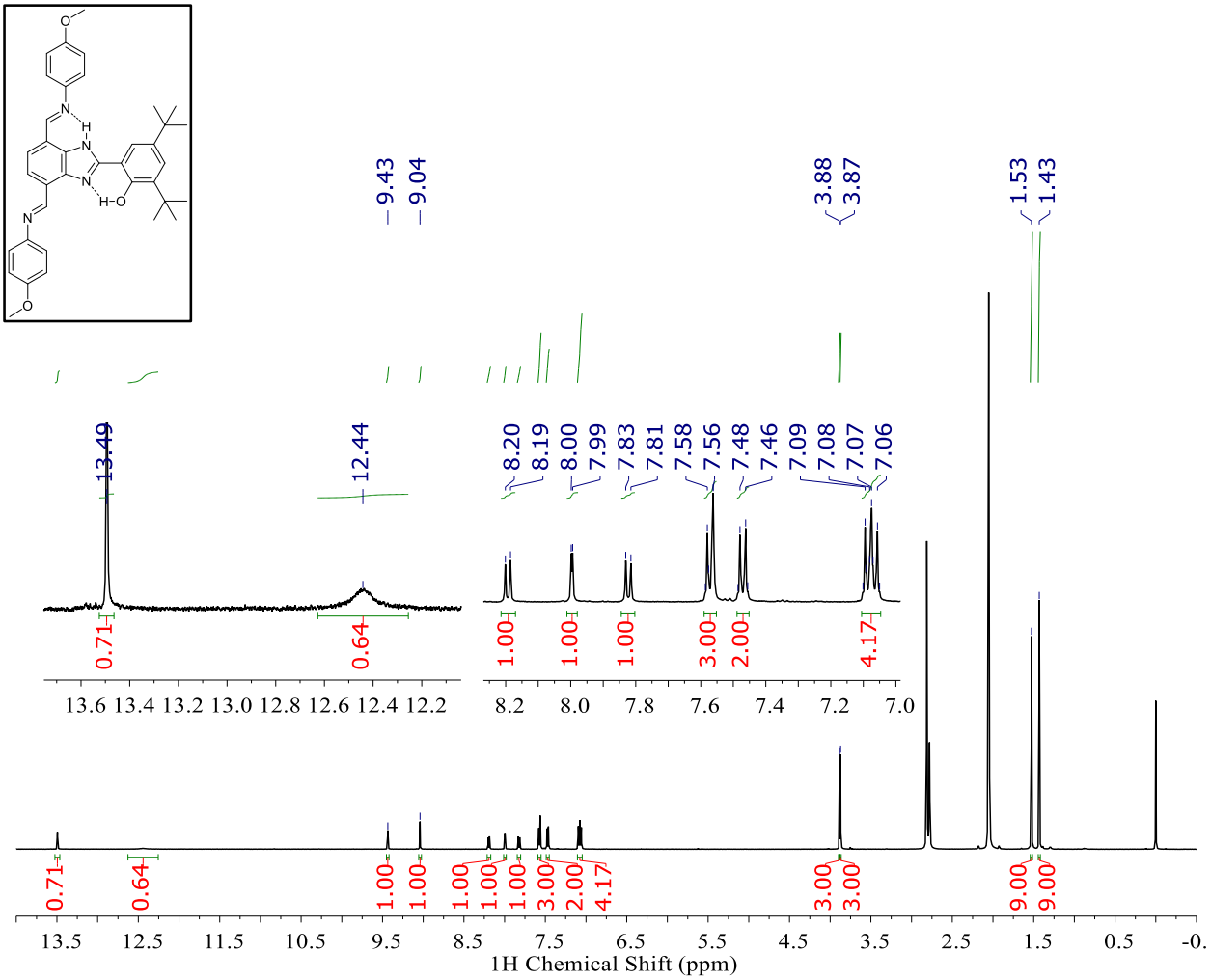

Figure S13. 500 MHz ^{1}H NMR spectrum of **3** in $(CD_3)_2CO$.

Compound **3**

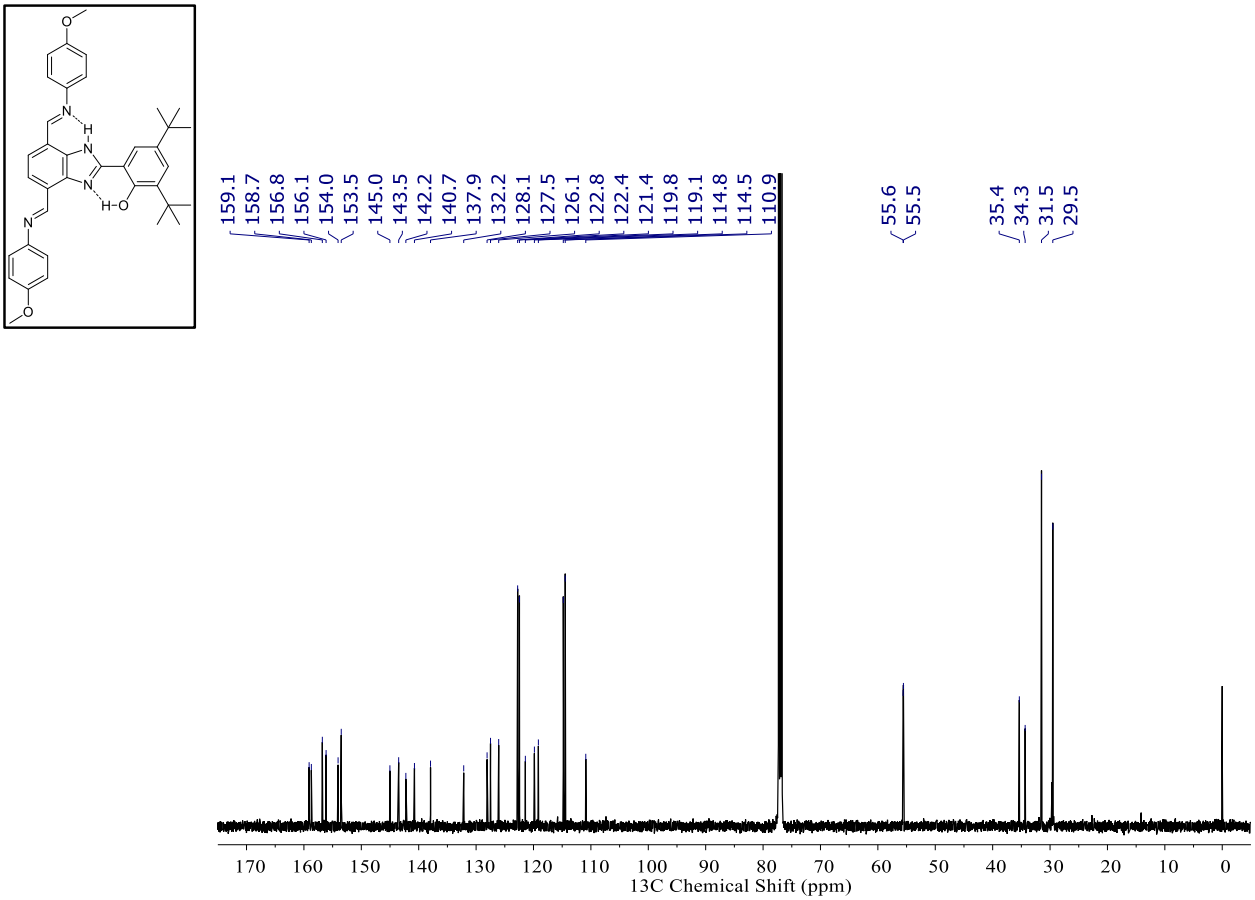

Figure S14. 126 MHz ^{13}C NMR spectrum of **3** in $CDCl_3$.

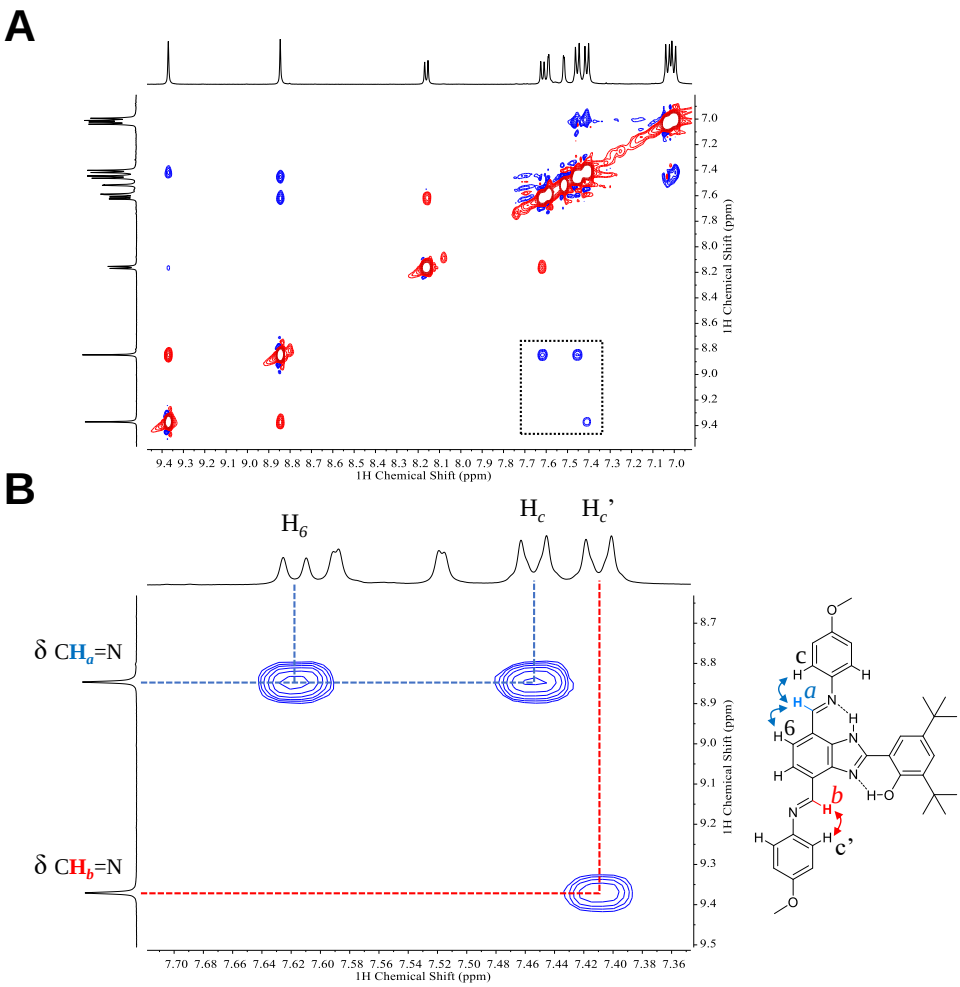

Figure S15. **(A)** NOESY experiment of **3** in CD_2Cl_2 showing the downfield/aromatic regions of the spectrum. **(B)** Expansion of the selected area (dotted rectangle) in **A**. The arrows shown in the molecular structure describe the interactions through the space of the azomethine protons (H_a and H_b) of both TPA branches (color coded).

1.4. Crystal Structure and X-Ray Data for Compound 3

A clear light-yellow thin needle-like specimen of $C_{37}H_{40}N_4O_3$, approximate dimensions 0.026 mm x 0.086 mm x 0.884 mm, was used for the X-ray crystallographic analysis. The X-ray intensity data were measured.

Table S1. Data collection details for **3**.

Axis	dx/mm	2θ/°	ω/°	φ/°	χ/°	Width/°	Frames	Time/s	Wavelength/Å	Voltage/kV	Current/mA	Temperature/K
Omega	50.568	-34.00	-34.00	0.00	54.80	0.50	364	120.00	0.71073	50	30.0	n/a
Omega	50.568	-34.00	-34.00	120.00	54.80	0.50	364	120.00	0.71073	50	30.0	n/a
Omega	50.568	-34.00	-34.00	240.00	54.80	0.50	364	120.00	0.71073	50	30.0	n/a

A total of 1092 frames were collected. The total exposure time was 36.40 hours. The frames were integrated with the Bruker SAINT software package using a narrow-frame algorithm. The integration of the data using a monoclinic unit cell yielded a total of 25976 reflections to a maximum θ angle of 25.52° (0.82 Å resolution), of which 6081 were independent (average redundancy 4.272, completeness = 99.4%, R_{int} = 10.68%, R_{sig} = 9.31%) and 3963 (65.17%) were greater than $2\sigma(F^2)$. The final cell constants of a = 33.507(8) Å, b = 7.0694(18) Å, c = 32.051(12) Å, β = 120.434(4)°, volume = 6546.(3) $Å^3$, are based upon the refinement of the XYZ-centroids of 2089 reflections above 20 σ(I) with 5.086° < 2θ < 50.01°. Data were corrected for absorption effects using the multi-scan method (SADABS). The ratio of minimum to maximum apparent transmission was 0.645. The calculated minimum and maximum transmission coefficients (based on crystal size) are 0.9350 and 0.9980. The structure was solved and refined using the Bruker SHELXTL Software Package, using the space group C 1 2/c 1, with Z = 8 for the formula unit, $C_{37}H_{40}N_4O_3$. The final anisotropic full-matrix least-squares refinement on F^2 with 406 variables converged at R1 = 7.91%, for the observed data and wR2 = 16.96% for all data. The goodness-of-fit was 1.069. The largest peak in the final difference electron density synthesis was 0.296 $e^-/Å^3$ and the largest hole was -0.201 $e^-/Å^3$ with an RMS deviation of 0.063 $e^-/Å^3$. On the basis of the final model, the calculated density was 1.195 g/cm^3 and F(000), 2512 e^-.

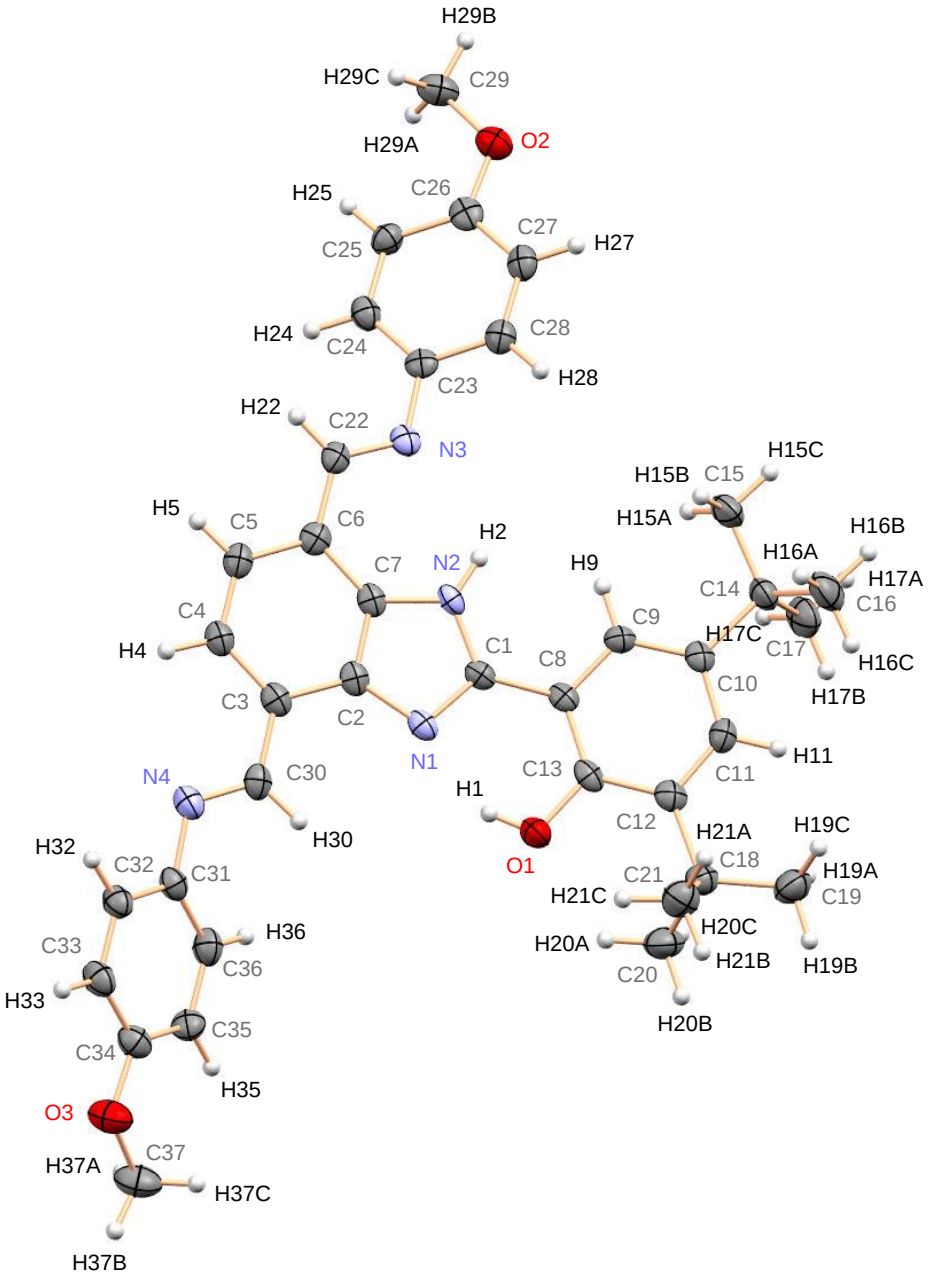

Figure S16. ORTEP representation of the crystal structure of **3**. Carbons are shown in grey, oxygens in red, nitrogens in light violet and hydrogens in white. Thermal ellipsoids are drawn at the 50% probability level.

Table S2. Sample and crystal data for **3**.

Identification code	Odella_BIP_diimine_methoxy	
Chemical formula	$C_{37}H_{40}N_4O_3$	
Formula weight	588.73 g/mol	
Temperature	123(0) K	
Wavelength	0.71073 Å	
Crystal size	0.026 x 0.086 x 0.884 mm	
Crystal habit	clear light yellow thin needle	
Crystal system	monoclinic	
Space group	C 1 2/c 1	
Unit cell dimensions	a = 33.507(8) Å	α = 90°
	b = 7.0694(18) Å	β = 120.434(4)°
	c = 32.051(12) Å	γ = 90°
Volume	6546.(3) $Å^3$	
Z	8	
Density (calculated)	1.195 g/cm^3	
Absorption coefficient	0.077 mm^{-1}	
F(000)	2512	

Table S3. Data collection and structure refinement for **3**.

Theta range for data collection	2.43 to 25.52°
Index ranges	-40<=h<=40, -8<=k<=8, -38<=l<=38
Reflections collected	25976
Independent reflections	6081 [R(int) = 0.1068]
Coverage of independent reflections	99.4%
Absorption correction	multi-scan
Max. and min. transmission	0.9980 and 0.9350
Structure solution technique	direct methods
Structure solution program	SHELXTL XT-2014/4
Refinement method	Full-matrix least-squares on F^2
Refinement program	SHELXL-2014/7 (Sheldrick, 2014)
Function minimized	$\Sigma\, w(F_o^2 - F_c^2)^2$
Data / restraints / parameters	6081 / 0 / 406
Goodness-of-fit on F^2	1.069
Final R indices	3963 data; I>2σ(I) R1 = 0.0791, wR2 = 0.1517
	all data R1 = 0.1239, wR2 = 0.1696
Weighting scheme	$w=1/[\sigma^2(F_o^2)+(0.0520P)^2+5.4931P]$ where $P=(F_o^2+2F_c^2)/3$
Largest diff. peak and hole	0.296 and -0.201 eÅ^{-3}
R.M.S. deviation from mean	0.063 eÅ^{-3}

Table S4. Atomic coordinates and equivalent isotropic atomic displacement parameters ($Å^2$) for **3**. U(eq) is defined as one third of the trace of the orthogonalized U_{ij} tensor.

	x/a	y/b	z/c	U(eq)
O1	0.32628(7)	0.6581(3)	0.44946(7)	0.0316(6)
O2	0.29586(8)	0.3844(3)	0.80170(7)	0.0357(6)
O3	0.08408(9)	0.5875(3)	0.14933(8)	0.0457(7)
N1	0.26040(8)	0.5534(3)	0.46536(8)	0.0245(6)
N2	0.27580(8)	0.5040(3)	0.54055(8)	0.0224(6)
N3	0.24794(9)	0.4110(3)	0.60786(9)	0.0261(6)
N4	0.12683(9)	0.4449(4)	0.33839(9)	0.0294(6)
C1	0.29300(10)	0.5586(4)	0.51205(10)	0.0205(7)
C2	0.22077(10)	0.4880(4)	0.46427(11)	0.0230(7)
C3	0.17599(10)	0.4517(4)	0.42453(11)	0.0252(7)
C4	0.14299(11)	0.3855(4)	0.43529(11)	0.0257(7)
C5	0.15310(10)	0.3550(4)	0.48230(11)	0.0268(7)
C6	0.19719(10)	0.3909(4)	0.52228(11)	0.0244(7)
C7	0.22999(10)	0.4583(4)	0.51129(10)	0.0226(7)
C8	0.34118(10)	0.6097(4)	0.53027(10)	0.0215(7)
C9	0.37321(10)	0.6030(4)	0.58013(10)	0.0234(7)
C10	0.41937(10)	0.6385(4)	0.59837(11)	0.0240(7)
C11	0.43333(10)	0.6842(4)	0.56522(11)	0.0265(7)
C12	0.40384(11)	0.6914(4)	0.51544(11)	0.0262(7)
C13	0.35647(10)	0.6543(4)	0.49803(11)	0.0250(7)
C14	0.45571(11)	0.6288(5)	0.65297(11)	0.0311(8)
C15	0.43417(12)	0.5625(5)	0.68241(11)	0.0382(9)

	x/a	y/b	z/c	U(eq)
C16	0.49350(12)	0.4856(6)	0.66031(13)	0.0468(10)
C17	0.47723(12)	0.8246(5)	0.67077(12)	0.0443(10)
C18	0.42238(11)	0.7307(5)	0.48126(12)	0.0318(8)
C19	0.47485(12)	0.7626(5)	0.50865(13)	0.0423(9)
C20	0.39974(13)	0.9085(5)	0.45049(13)	0.0424(9)
C21	0.41214(12)	0.5608(5)	0.44760(13)	0.0409(9)
C22	0.20819(11)	0.3642(4)	0.57203(11)	0.0255(7)
C23	0.25645(11)	0.3990(4)	0.65555(11)	0.0250(7)
C24	0.22323(11)	0.4244(4)	0.66898(11)	0.0292(8)
C25	0.23483(11)	0.4196(4)	0.71734(11)	0.0294(8)
C26	0.28052(11)	0.3889(4)	0.75339(11)	0.0282(7)
C27	0.31396(11)	0.3628(4)	0.74049(11)	0.0297(8)
C28	0.30225(11)	0.3709(4)	0.69254(11)	0.0275(7)
C29	0.26246(12)	0.4024(5)	0.81628(12)	0.0378(9)
C30	0.16620(10)	0.4829(4)	0.37521(11)	0.0268(7)
C31	0.11861(10)	0.4875(4)	0.29154(11)	0.0278(7)
C32	0.08748(11)	0.3744(5)	0.25316(11)	0.0303(8)
C33	0.07741(11)	0.4076(5)	0.20687(12)	0.0341(8)
C34	0.09742(11)	0.5624(5)	0.19706(11)	0.0325(8)
C35	0.12717(11)	0.6800(5)	0.23439(11)	0.0319(8)
C36	0.13783(11)	0.6414(5)	0.28099(12)	0.0331(8)
C37	0.09939(14)	0.7550(5)	0.13743(13)	0.0483(10)

Table S5. Bond lengths (Å) for **3**.

O1-C13	1.361(3)	O1-H1	0.84
O2-C26	1.362(4)	O2-C29	1.420(4)
O3-C34	1.370(4)	O3-C37	1.418(4)
N1-C1	1.334(4)	N1-C2	1.390(4)
N2-C1	1.360(4)	N2-C7	1.372(4)
N2-H2	0.88	N3-C22	1.286(4)
N3-C23	1.408(4)	N4-C30	1.276(4)
N4-C31	1.415(4)	C1-C8	1.457(4)
C2-C7	1.393(4)	C2-C3	1.415(4)
C3-C4	1.395(4)	C3-C30	1.460(4)
C4-C5	1.384(4)	C4-H4	0.95
C5-C6	1.404(4)	C5-H5	0.95
C6-C7	1.396(4)	C6-C22	1.456(4)
C8-C13	1.402(4)	C8-C9	1.403(4)
C9-C10	1.372(4)	C9-H9	0.95
C10-C11	1.398(4)	C10-C14	1.546(4)
C11-C12	1.388(4)	C11-H11	0.95
C12-C13	1.415(4)	C12-C18	1.534(4)
C14-C15	1.523(4)	C14-C17	1.531(5)
C14-C16	1.543(5)	C15-H15A	0.98
C15-H15B	0.98	C15-H15C	0.98
C16-H16A	0.98	C16-H16B	0.98
C16-H16C	0.98	C17-H17A	0.98

C17-H17B	0.98	C17-H17C	0.98
C18-C19	1.533(5)	C18-C21	1.533(5)
C18-C20	1.539(5)	C19-H19A	0.98
C19-H19B	0.98	C19-H19C	0.98
C20-H20A	0.98	C20-H20B	0.98
C20-H20C	0.98	C21-H21A	0.98
C21-H21B	0.98	C21-H21C	0.98
C22-H22	0.95	C23-C24	1.393(4)
C23-C28	1.399(4)	C24-C25	1.394(4)
C24-H24	0.95	C25-C26	1.391(4)
C25-H25	0.95	C26-C27	1.389(4)
C27-C28	1.381(4)	C27-H27	0.95
C28-H28	0.95	C29-H29A	0.98
C29-H29B	0.98	C29-H29C	0.98
C30-H30	0.95	C31-C36	1.391(4)
C31-C32	1.393(4)	C32-C33	1.365(4)
C32-H32	0.95	C33-C34	1.400(5)
C33-H33	0.95	C34-C35	1.381(4)
C35-C36	1.376(4)	C35-H35	0.95
C36-H36	0.95	C37-H37A	0.98
C37-H37B	0.98	C37-H37C	0.98

Table S6. Bond angles (°) for **3**.

C13-O1-H1	109.5	C26-O2-C29	117.7(3)
C34-O3-C37	116.8(3)	C1-N1-C2	105.5(2)
C1-N2-C7	108.4(2)	C1-N2-H2	125.8
C7-N2-H2	125.8	C22-N3-C23	120.2(3)
C30-N4-C31	119.4(3)	N1-C1-N2	111.2(3)
N1-C1-C8	124.6(3)	N2-C1-C8	124.2(2)
N1-C2-C7	109.7(3)	N1-C2-C3	130.3(3)
C7-C2-C3	120.0(3)	C4-C3-C2	116.8(3)
C4-C3-C30	123.2(3)	C2-C3-C30	120.1(3)
C5-C4-C3	122.3(3)	C5-C4-H4	118.9
C3-C4-H4	118.9	C4-C5-C6	122.0(3)
C4-C5-H5	119.0	C6-C5-H5	119.0
C7-C6-C5	115.5(3)	C7-C6-C22	121.7(3)
C5-C6-C22	122.8(3)	N2-C7-C2	105.2(3)
N2-C7-C6	131.2(3)	C2-C7-C6	123.6(3)
C13-C8-C9	119.5(3)	C13-C8-C1	120.3(3)
C9-C8-C1	120.1(3)	C10-C9-C8	121.7(3)
C10-C9-H9	119.1	C8-C9-H9	119.1
C9-C10-C11	117.2(3)	C9-C10-C14	123.1(3)
C11-C10-C14	119.7(3)	C12-C11-C10	124.4(3)
C12-C11-H11	117.8	C10-C11-H11	117.8
C11-C12-C13	116.7(3)	C11-C12-C18	121.2(3)
C13-C12-C18	122.1(3)	O1-C13-C8	120.7(3)

O1-C13-C12	118.9(3)	C8-C13-C12	120.4(3)
C15-C14-C17	109.2(3)	C15-C14-C16	108.3(3)
C17-C14-C16	109.9(3)	C15-C14-C10	111.5(3)
C17-C14-C10	109.5(3)	C16-C14-C10	108.4(3)
C14-C15-H15A	109.5	C14-C15-H15B	109.5
H15A-C15-H15B	109.5	C14-C15-H15C	109.5
H15A-C15-H15C	109.5	H15B-C15-H15C	109.5
C14-C16-H16A	109.5	C14-C16-H16B	109.5
H16A-C16-H16B	109.5	C14-C16-H16C	109.5
H16A-C16-H16C	109.5	H16B-C16-H16C	109.5
C14-C17-H17A	109.5	C14-C17-H17B	109.5
H17A-C17-H17B	109.5	C14-C17-H17C	109.5
H17A-C17-H17C	109.5	H17B-C17-H17C	109.5
C19-C18-C21	107.6(3)	C19-C18-C12	112.3(3)
C21-C18-C12	109.5(3)	C19-C18-C20	107.3(3)
C21-C18-C20	109.1(3)	C12-C18-C20	111.0(3)
C18-C19-H19A	109.5	C18-C19-H19B	109.5
H19A-C19-H19B	109.5	C18-C19-H19C	109.5
H19A-C19-H19C	109.5	H19B-C19-H19C	109.5
C18-C20-H20A	109.5	C18-C20-H20B	109.5
H20A-C20-H20B	109.5	C18-C20-H20C	109.5
H20A-C20-H20C	109.5	H20B-C20-H20C	109.5
C18-C21-H21A	109.5	C18-C21-H21B	109.5
H21A-C21-H21B	109.5	C18-C21-H21C	109.5

H21A-C21-H21C	109.5	H21B-C21-H21C	109.5
N3-C22-C6	121.2(3)	N3-C22-H22	119.4
C6-C22-H22	119.4	C24-C23-C28	117.5(3)
C24-C23-N3	125.0(3)	C28-C23-N3	117.4(3)
C23-C24-C25	121.6(3)	C23-C24-H24	119.2
C25-C24-H24	119.2	C26-C25-C24	119.8(3)
C26-C25-H25	120.1	C24-C25-H25	120.1
O2-C26-C27	116.0(3)	O2-C26-C25	124.8(3)
C27-C26-C25	119.2(3)	C28-C27-C26	120.5(3)
C28-C27-H27	119.7	C26-C27-H27	119.7
C27-C28-C23	121.4(3)	C27-C28-H28	119.3
C23-C28-H28	119.3	O2-C29-H29A	109.5
O2-C29-H29B	109.5	H29A-C29-H29B	109.5
O2-C29-H29C	109.5	H29A-C29-H29C	109.5
H29B-C29-H29C	109.5	N4-C30-C3	122.0(3)
N4-C30-H30	119.0	C3-C30-H30	119.0
C36-C31-C32	117.8(3)	C36-C31-N4	124.0(3)
C32-C31-N4	118.1(3)	C33-C32-C31	121.6(3)
C33-C32-H32	119.2	C31-C32-H32	119.2
C32-C33-C34	119.7(3)	C32-C33-H33	120.1
C34-C33-H33	120.1	O3-C34-C35	125.0(3)
O3-C34-C33	115.4(3)	C35-C34-C33	119.6(3)
C36-C35-C34	119.9(3)	C36-C35-H35	120.1
C34-C35-H35	120.1	C35-C36-C31	121.5(3)

C35-C36-H36	119.3	C31-C36-H36	119.3
O3-C37-H37A	109.5	O3-C37-H37B	109.5
H37A-C37-H37B	109.5	O3-C37-H37C	109.5
H37A-C37-H37C	109.5	H37B-C37-H37C	109.5

Table S7. Torsion angles (°) for **3**.

C2-N1-C1-N2	-1.4(3)	C2-N1-C1-C8	176.7(3)
C7-N2-C1-N1	0.9(3)	C7-N2-C1-C8	-177.2(3)
C1-N1-C2-C7	1.4(3)	C1-N1-C2-C3	-178.8(3)
N1-C2-C3-C4	179.9(3)	C7-C2-C3-C4	-0.3(4)
N1-C2-C3-C30	0.1(5)	C7-C2-C3-C30	179.9(3)
C2-C3-C4-C5	-0.4(4)	C30-C3-C4-C5	179.3(3)
C3-C4-C5-C6	0.8(5)	C4-C5-C6-C7	-0.3(4)
C4-C5-C6-C22	178.4(3)	C1-N2-C7-C2	0.0(3)
C1-N2-C7-C6	178.4(3)	N1-C2-C7-N2	-0.9(3)
C3-C2-C7-N2	179.3(2)	N1-C2-C7-C6	-179.4(3)
C3-C2-C7-C6	0.8(4)	C5-C6-C7-N2	-178.6(3)
C22-C6-C7-N2	2.7(5)	C5-C6-C7-C2	-0.5(4)
C22-C6-C7-C2	-179.2(3)	N1-C1-C8-C13	-1.3(4)
N2-C1-C8-C13	176.4(3)	N1-C1-C8-C9	-177.3(3)
N2-C1-C8-C9	0.5(4)	C13-C8-C9-C10	-0.2(4)
C1-C8-C9-C10	175.8(3)	C8-C9-C10-C11	0.7(4)
C8-C9-C10-C14	-178.9(3)	C9-C10-C11-C12	-1.5(5)
C14-C10-C11-C12	178.1(3)	C10-C11-C12-C13	1.7(5)
C10-C11-C12-C18	-176.2(3)	C9-C8-C13-O1	178.7(3)
C1-C8-C13-O1	2.7(4)	C9-C8-C13-C12	0.3(4)
C1-C8-C13-C12	-175.7(3)	C11-C12-C13-O1	-179.4(3)
C18-C12-C13-O1	-1.6(4)	C11-C12-C13-C8	-1.0(4)
C18-C12-C13-C8	176.8(3)	C9-C10-C14-C15	3.9(4)

C11-C10-C14-C15	-175.6(3)	C9-C10-C14-C17	-117.0(3)
C11-C10-C14-C17	63.4(4)	C9-C10-C14-C16	123.0(3)
C11-C10-C14-C16	-56.6(4)	C11-C12-C18-C19	-1.1(4)
C13-C12-C18-C19	-178.8(3)	C11-C12-C18-C21	118.3(3)
C13-C12-C18-C21	-59.4(4)	C11-C12-C18-C20	-121.2(3)
C13-C12-C18-C20	61.1(4)	C23-N3-C22-C6	174.6(3)
C7-C6-C22-N3	3.6(4)	C5-C6-C22-N3	-175.1(3)
C22-N3-C23-C24	-31.0(4)	C22-N3-C23-C28	153.1(3)
C28-C23-C24-C25	-0.9(5)	N3-C23-C24-C25	-176.7(3)
C23-C24-C25-C26	0.0(5)	C29-O2-C26-C27	-177.4(3)
C29-O2-C26-C25	3.5(4)	C24-C25-C26-O2	178.9(3)
C24-C25-C26-C27	-0.2(5)	O2-C26-C27-C28	-177.9(3)
C25-C26-C27-C28	1.3(5)	C26-C27-C28-C23	-2.2(5)
C24-C23-C28-C27	2.0(4)	N3-C23-C28-C27	178.1(3)
C31-N4-C30-C3	176.7(3)	C4-C3-C30-N4	-2.6(5)
C2-C3-C30-N4	177.2(3)	C30-N4-C31-C36	-33.2(4)
C30-N4-C31-C32	150.3(3)	C36-C31-C32-C33	2.6(5)
N4-C31-C32-C33	179.4(3)	C31-C32-C33-C34	-2.2(5)
C37-O3-C34-C35	-5.1(5)	C37-O3-C34-C33	172.8(3)
C32-C33-C34-O3	-178.0(3)	C32-C33-C34-C35	0.0(5)
O3-C34-C35-C36	179.5(3)	C33-C34-C35-C36	1.7(5)
C34-C35-C36-C31	-1.2(5)	C32-C31-C36-C35	-0.9(5)
N4-C31-C36-C35	-177.5(3)		

Table S8. Anisotropic atomic displacement parameters ($Å^2$) for **3**.

The anisotropic atomic displacement factor exponent takes the form: -2π2[h2 a*2 U11 + ... + 2 h k a* b* U12]

	U_{11}	U_{22}	U_{33}	U_{23}	U_{13}	U_{12}
O1	0.0290(12)	0.0378(14)	0.0244(12)	0.0024(10)	0.0108(10)	0.0026(11)
O2	0.0398(14)	0.0349(14)	0.0295(13)	-0.0008(10)	0.0154(11)	0.0005(11)
O3	0.0609(17)	0.0392(16)	0.0349(14)	0.0040(12)	0.0228(13)	-0.0035(13)
N1	0.0264(14)	0.0183(14)	0.0228(14)	0.0000(11)	0.0081(12)	0.0028(11)
N2	0.0214(14)	0.0194(14)	0.0191(12)	-0.0004(11)	0.0049(11)	0.0043(11)
N3	0.0269(15)	0.0191(14)	0.0284(14)	0.0031(11)	0.0111(13)	0.0021(11)
N4	0.0271(15)	0.0249(15)	0.0269(14)	0.0001(12)	0.0068(13)	0.0004(12)
C1	0.0270(17)	0.0133(15)	0.0194(15)	-0.0016(12)	0.0104(14)	0.0045(12)
C2	0.0241(17)	0.0131(15)	0.0288(17)	-0.0034(13)	0.0113(14)	0.0056(13)
C3	0.0274(18)	0.0168(16)	0.0273(17)	-0.0018(13)	0.0109(15)	0.0054(13)
C4	0.0244(17)	0.0181(16)	0.0288(17)	-0.0027(13)	0.0093(15)	0.0022(13)
C5	0.0247(17)	0.0176(17)	0.0368(19)	-0.0019(14)	0.0146(15)	0.0009(13)
C6	0.0283(18)	0.0139(15)	0.0327(17)	-0.0015(13)	0.0168(15)	0.0049(13)
C7	0.0237(17)	0.0127(15)	0.0272(16)	-0.0023(13)	0.0098(14)	0.0045(12)
C8	0.0266(17)	0.0120(15)	0.0230(15)	0.0007(12)	0.0104(14)	0.0033(12)
C9	0.0292(18)	0.0180(16)	0.0261(16)	0.0019(13)	0.0163(15)	0.0034(13)
C10	0.0257(17)	0.0148(16)	0.0290(17)	0.0030(13)	0.0120(15)	0.0054(13)
C11	0.0229(17)	0.0201(17)	0.0360(18)	-0.0006(14)	0.0144(15)	0.0009(13)
C12	0.0310(19)	0.0174(16)	0.0308(18)	0.0036(14)	0.0161(15)	0.0079(14)
C13	0.0267(18)	0.0165(16)	0.0248(16)	0.0016(13)	0.0080(15)	0.0077(13)
C14	0.0256(18)	0.036(2)	0.0236(16)	0.0014(15)	0.0062(15)	0.0008(15)

	U_{11}	U_{22}	U_{33}	U_{23}	U_{13}	U_{12}
C15	0.034(2)	0.046(2)	0.0224(17)	0.0024(16)	0.0057(16)	-0.0038(17)
C16	0.036(2)	0.058(3)	0.035(2)	0.0095(19)	0.0098(18)	0.0169(19)
C17	0.036(2)	0.047(2)	0.0339(19)	-0.0054(18)	0.0061(17)	-0.0126(18)
C18	0.034(2)	0.0301(19)	0.0353(19)	0.0060(15)	0.0207(16)	0.0059(15)
C19	0.042(2)	0.047(2)	0.048(2)	0.0055(19)	0.0305(19)	0.0022(18)
C20	0.050(2)	0.043(2)	0.044(2)	0.0130(18)	0.0312(19)	0.0098(18)
C21	0.043(2)	0.042(2)	0.042(2)	-0.0019(18)	0.0250(19)	0.0047(18)
C22	0.0245(17)	0.0180(16)	0.0343(18)	0.0032(14)	0.0153(16)	0.0048(13)
C23	0.0317(18)	0.0132(15)	0.0309(17)	0.0008(13)	0.0163(16)	-0.0011(13)
C24	0.0267(18)	0.0243(18)	0.0308(18)	0.0003(14)	0.0103(15)	0.0013(14)
C25	0.0303(19)	0.0280(19)	0.0341(18)	0.0002(15)	0.0194(16)	0.0021(15)
C26	0.0336(19)	0.0122(16)	0.0347(18)	-0.0001(14)	0.0144(16)	-0.0020(13)
C27	0.0268(18)	0.0216(18)	0.0351(19)	-0.0020(14)	0.0116(16)	-0.0015(14)
C28	0.0272(18)	0.0201(17)	0.0345(18)	-0.0018(14)	0.0151(15)	0.0003(13)
C29	0.051(2)	0.034(2)	0.0317(18)	0.0029(16)	0.0234(18)	0.0047(17)
C30	0.0227(18)	0.0203(17)	0.0353(18)	-0.0021(14)	0.0132(16)	0.0036(13)
C31	0.0245(18)	0.0263(18)	0.0280(17)	0.0009(14)	0.0101(15)	0.0059(14)
C32	0.0283(18)	0.0264(18)	0.0296(18)	0.0024(15)	0.0099(15)	-0.0011(14)
C33	0.033(2)	0.030(2)	0.0296(18)	-0.0017(15)	0.0088(16)	-0.0026(15)
C34	0.035(2)	0.029(2)	0.0304(18)	0.0020(15)	0.0145(16)	0.0062(15)
C35	0.0345(19)	0.0248(18)	0.0363(19)	0.0036(15)	0.0179(16)	-0.0023(15)
C36	0.0269(19)	0.0292(19)	0.0377(19)	-0.0031(16)	0.0123(16)	-0.0025(15)
C37	0.068(3)	0.037(2)	0.042(2)	0.0109(18)	0.029(2)	0.005(2)

Table S9. Hydrogen atomic coordinates and isotropic atomic displacement parameters ($Å^2$) for **3**.

	x/a	y/b	z/c	U(eq)
H1	0.2993	0.6377	0.4440	0.047
H2	0.2914	0.4989	0.5724	0.027
H4	0.1125	0.3606	0.4094	0.031
H5	0.1295	0.3083	0.4877	0.032
H9	0.3626	0.5731	0.6018	0.028
H11	0.4651	0.7121	0.5776	0.032
H15A	0.4583	0.5528	0.7166	0.057
H15B	0.4198	0.4384	0.6707	0.057
H15C	0.4106	0.6537	0.6789	0.057
H16A	0.5171	0.4792	0.6947	0.07
H16B	0.5079	0.5262	0.6417	0.07
H16C	0.4795	0.3604	0.6491	0.07
H17A	0.4533	0.9137	0.6671	0.067
H17B	0.4908	0.8686	0.6516	0.067
H17C	0.5014	0.8169	0.7049	0.067
H19A	0.4824	0.8726	0.5300	0.063
H19B	0.4852	0.7854	0.4854	0.063
H19C	0.4905	0.6504	0.5280	0.063
H20A	0.3660	0.8939	0.4329	0.064
H20B	0.4104	0.9252	0.4273	0.064
H20C	0.4084	1.0195	0.4716	0.064
H21A	0.4263	0.4470	0.4670	0.061

	x/a	y/b	z/c	U(eq)
H21B	0.4249	0.5841	0.4265	0.061
H21C	0.3786	0.5428	0.4278	0.061
H22	0.1856	0.3112	0.5781	0.031
H24	0.1919	0.4455	0.6446	0.035
H25	0.2116	0.4373	0.7256	0.035
H27	0.3451	0.3392	0.7648	0.036
H28	0.3258	0.3572	0.6845	0.033
H29A	0.2473	0.5261	0.8062	0.057
H29B	0.2778	0.3913	0.8516	0.057
H29C	0.2392	0.3021	0.8012	0.057
H30	0.1899	0.5332	0.3704	0.032
H32	0.0729	0.2717	0.2593	0.036
H33	0.0569	0.3261	0.1814	0.041
H35	0.1402	0.7873	0.2279	0.038
H36	0.1588	0.7217	0.3065	0.04
H37A	0.0888	0.8654	0.1477	0.073
H37B	0.0866	0.7603	0.1024	0.073
H37C	0.1333	0.7552	0.1540	0.073

Table S10. Hydrogen bond distances (Å) and angles (°) for **3**.

	Donor-H	**Acceptor-H**	**Donor-Acceptor**	**Angle**
O1-H1···N1	0.84	1.85	2.611(3)	149.5
N2-H2···N3	0.88	2.34	2.829(4)	115.0

2. Computational Methods

Electronic structure calculations were performed with density functional theory (DFT) using the B3LYP functional[5,6] with dispersion corrections (D3(BJ))[7–9] and the 6-31G** basis set.[10–13] Geometry optimizations and free energy calculations were performed in dichloromethane solution using the conductor-like polarizable continuum model (CPCM).[14,15] The Bondi atomic radii were used, and nonelectrostatic contributions of dispersion, repulsion, and cavitation energies were included.[16–18] Previous benchmarking of this level of theory has shown that it performs well for similar systems.[2,19] The Gaussian16 electronic structure program was used for all DFT calculations.[20] Free energies were calculated using the standard Gibbs relation, $\Delta G_0 = \Delta H_0 - T\Delta S_0$, at T = 298.15 K and included zero-point energy, entropic contributions, and solvation effects.

Relative free energies were calculated for all protonation states of selected rotamers. These rotamers and states are shown in Figures 5A and B in the main manuscript for compounds **2** and **3**, respectively. All calculated relative free energies were referenced to the lowest energy rotamer/protonation state of each neutral or oxidized compound. The Boltzmann populations were computed using Eq. 1 in the main manuscript. The calculated relative free energies and populations of each state are given in Table S11 and Table S12.

The redox potentials were computed from the corresponding reaction free energies using an experimentally known reference potential within a thermodynamic cycle. The reference potential used for computing the redox potentials of compounds **1, G,** and **3** was the experimentally measured redox potential of 0.95 V vs SCE in dichloromethane of compound **2**. In previous studies,[19] these methods have produced accurate and predictive results in agreement with experiments. The calculated redox potentials are reported in Table S13.

Computationally obtained IRSEC spectra for compounds **2** and **3** show the formation of the final E2PT products (Figure S17). Frequency calculations were performed for both the reduced (neutral) and oxidized (+1) species. To allow direct comparison with experimental IRSEC spectra, all computed frequencies were empirically scaled by a factor of 0.962 to match the experimental $C{=}NH^+$ protonated azomethine stretch at 1651 cm^{-1} of the E2PT product of compound **3**. To simulate line broadening, the peaks were dressed with an artificial Lorentzian function for a full-width-half-maximum (FWHM) of 12 cm^{-1}. Frequencies and characterization of selected vibrational modes are given in Table S14. Band assignments were performed by visually inspecting displacements along the computed normal mode of each vibration. These computational

IRSEC results are in good agreement with experimentally obtained IRSEC spectra (Figure 8). Spin densities for the E0PT and E2PT products of compounds **2** and **3** were also produced and plotted (Figure S18).

Table S11. Relative Free Energies and Populations of compound **2**.[a]

	Proton Positions[a]		Relative Free Energies[b]		Populations[c]	
	Phenolic	Benzimidazole	Neutral	Oxidized	Neutral	Oxidized
Rotamer A	1	1	3.76	13.36	0.16%	0.00%
	2	1	5.57	5.20	0.01%	0.01%
	3	1	16.96	6.07	0.00%	0.00%
Rotamer B	1	1	2.56	12.78	1.21%	0.00%
	2	1	9.20	9.59	0.00%	0.00%
Rotamer C	1	1	0.00	13.44	98.58%	0.00%
	1	2	5.18	11.58	0.01%	0.00%
	2	1	4.69	4.31	0.03%	0.06%
	2	2	7.99	0.00	0.00%	99.92%
Rotamer D	1	1	5.64	17.57	0.01%	0.00%
	2	1	10.24	11.56	0.00%	0.00%

[a]See Figure 5A for rotamers and proton positions.
[b]Relative free energies reported in kcal/mol.
[c]Populations reported in percentages.

Table S12. Relative Free Energies and Populations of compound **3**.[a]

	Proton Position[a]		Relative Free Energies[b]		Populations[c]	
	Phenolic	Benzimidazole	Neutral	Oxidized	Neutral	Oxidized
Rotamer A	1	1	0.57	11.82	27.02%	0.00%
	1	2	5.94	13.37	0.00%	0.00%
	2	1	2.5	2.22	0.98%	2.15%
	2	2	5.79	0	0.00%	97.47%
	3	1	13.7	5.38	0.00%	0.01%
	3	2	19.69	9.57	0.00%	0.00%
Rotamer B	1	1	6.11	16.88	0.00%	0.00%
	2	1	8.68	10.53	0.00%	0.00%
	3	1	17.67	11.09	0.00%	0.00%
Rotamer C	1	1	0	9.77	71.93%	0.00%
	1	2	4.58	12.48	0.03%	0.00%
	2	1	5.25	7.17	0.01%	0.00%
	2	2	7.06	3.25	0.00%	0.37%
Rotamer D	1	1	4.87	15.22	0.02%	0.00%
	2	1	9.39	14.52	0.00%	0.00%

[a]See Figure 5B for rotamers and proton positions.
[b]Relative free energies reported in kcal/mol.
[c]Populations reported in percentages.

Table S13. Calculated Redox Potentials.[a]

	E0PT	E1PT	E2PT
Compound **1**	1.52	1.14	N/A[b]
Compound **G**	1.63	1.25	N/A[c]
Compound **2**	1.54	1.14	0.95[d]
Compound **3**	1.26	0.92	0.84

[a]Redox potentials reported in V vs SCE.

[b]Compound **1** cannot have an E2PT product.

[c]Compound **G** does not have a minimum corresponding to the E2PT product.

[d]This redox potential was used as reference and agrees with experiment by construction.

Table S14. Peak Assignment of Computational IRSEC.

Compound	State	Freq.[a]	Peak Description
2	E2PT	1560	breathing mode of TPA
	"	1566	breathing mode of phenol
	"	1651	protonated azomethine stretch
3	E1PT	1532	breathing mode of benzimidazole
	"	1544	bend mode of benzimidazole proton on benzimidazole donor
	"	1570	breathing mode of phenol
	"	1575	breathing mode of TPA
3	E2PT	1537	breathing mode of TPA
	"	1560	breathing mode of TPA
	"	1570	breathing mode of phenol
	"	1593	breathing mode of TPA with azomethine bending
	"	1651	protonated azomethine stretch

[a]Computationally obtained vibrational frequencies reported in cm^{-1}.

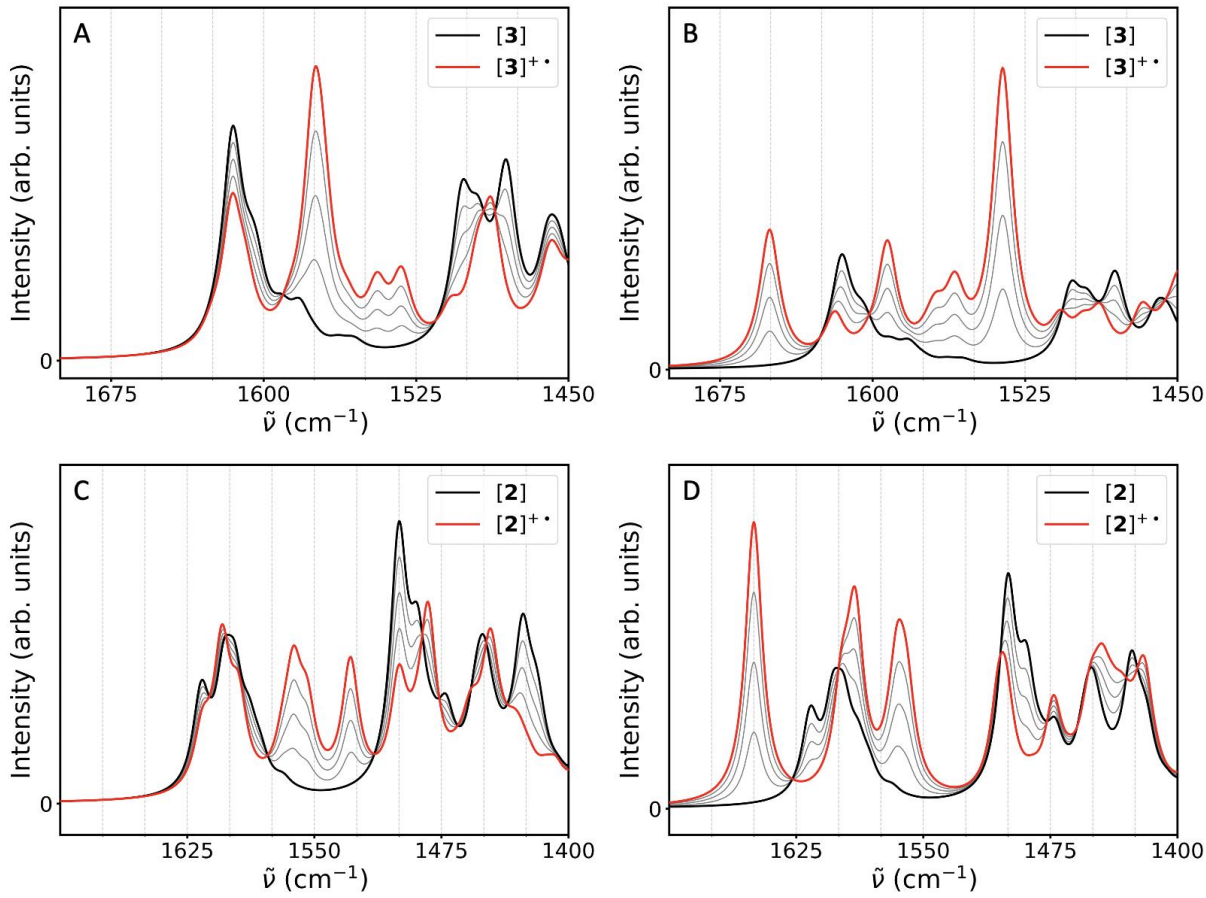

Figure S17. Computationally produced IRSEC spectra. The bold black lines show the spectra of the reactant state of each compound, the bold red lines show the spectra of the product state, and the faded black lines show the simulated progression of the IRSEC as product is formed. Frame **A** shows the E1PT product of compound **3**. Frame **B** shows the E2PT product of compound **3**. Frame **C** shows the E1PT product of compound **2**. Frame **D** shows the E2PT product of compound **2**.

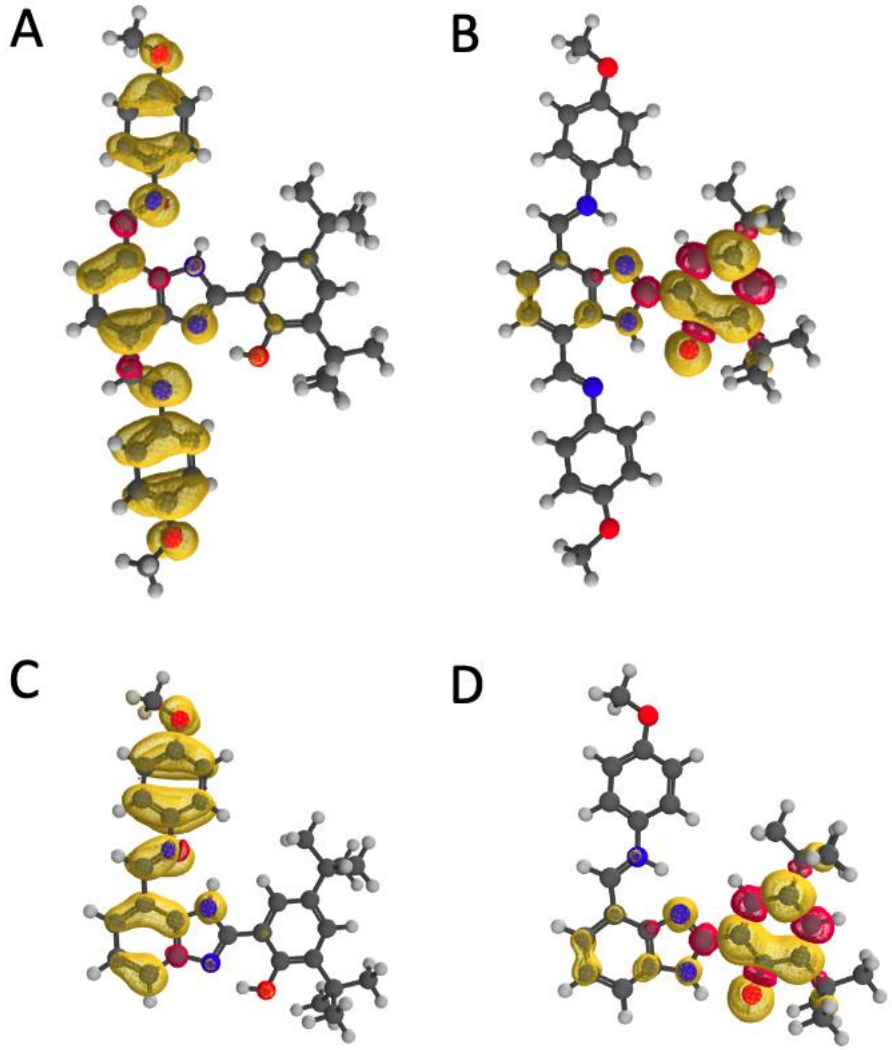

Figure S18. Spin density of hypothetical E0PT products and experimentally observed E2PT products of dominant rotamer species for compounds **2** and **3**. **(A)** E0PT product for **3**; **(B)** E2PT product for **3**; **(C)** E0PT product for **2**; **(D)** E2PT product for **2**. The substantial difference in the calculated redox potentials associated with the hypothetical E0PT products of **2** and **3** (Table S13) may be explained by the greater stabilization of the radical due to the more delocalized spin density of **3**. However, the similarity between the spin densities for the E2PT products of **2** and **3** indicates that this factor does not constitute an explanation for the differences in the experimentally measured redox potentials.

3. References

1 N. G. Connelly and W. E. Geiger, *Chem. Rev.*, 1996, **96**, 877–910.

2 E. Odella, S. J. Mora, B. L. Wadsworth, M. T. Huynh, J. J. Goings, P. A. Liddell, T. L. Groy, M. Gervaldo, L. E. Sereno, D. Gust, T. A. Moore, G. F. Moore, S. Hammes-Schiffer and A. L. Moore, *J. Am. Chem. Soc.*, 2018, **140**, 15450–15460.

3 J. M. Aslan, D. J. Boston and F. M. MacDonnell, *Chem. - A Eur. J.*, 2015, **21**, 17314–17323.

4 J. Shao, J. Chang and C. Chi, *Chem. – An Asian J.*, 2014, **9**, 253–260.

5 C. Lee, W. Yang and R. G. Parr, *Phys. Rev. B*, 1988, **37**, 785–789.

6 A. D. Becke, *J. Chem. Phys.*, 1993, **98**, 5648–5652.

7 P. J. Stephens, F. J. Devlin, C. S. Ashvar, C. F. Chabalowski and M. J. Frisch, *Faraday Discuss.*, 1994, **99**, 103–119.

8 S. Grimme, J. Antony, S. Ehrlich and H. Krieg, *J. Chem. Phys.*, 2010, **132**, 154104.

9 S. Grimme, S. Ehrlich and L. Goerigk, *J. Comput. Chem.*, 2011, **32**, 1456–1465.

10 R. Ditchfield, W. J. Hehre and J. A. Pople, *J. Chem. Phys.*, 1971, **54**, 724–728.

11 W. J. Hehre, R. Ditchfield and J. A. Pople, *J. Chem. Phys.*, 1972, **56**, 2257–2261.

12 P. C. Hariharan and J. A. Pople, *Theor. Chim. Acta*, 1973, **28**, 213–222.

13 M. M. Francl, W. J. Pietro, W. J. Hehre, J. S. Binkley, M. S. Gordon, D. J. DeFrees and J. A. Pople, *J. Chem. Phys.*, 1982, **77**, 3654–3665.

14 V. Barone and M. Cossi, *J. Phys. Chem. A*, 1998, **102**, 1995–2001.

15 M. Cossi, N. Rega, G. Scalmani and V. Barone, *J. Comput. Chem*, 2003, **24**, 669–681.

16 A. Bondi, *J. Phys. Chem.*, 1964, **68**, 441–451.

17 F. M. Floris, J. Tomasi and J. L. P. Ahuir, *J. Comput. Chem.*, 1991, **12**, 784–791.

18 R. A. Pierotti, *Chem. Rev.*, 1976, **76**, 717–726.

19 M. T. Huynh, S. J. Mora, M. Villalba, M. E. Tejeda-Ferrari, P. A. Liddell, B. R. Cherry, A.-L. Teillout, C. W. Machan, C. P. Kubiak, D. Gust, T. A. Moore, S. Hammes-Schiffer and A. L. Moore, *ACS Cent. Sci.*, 2017, **3**, 372–380.

20 M. J. Frisch, G. W. Trucks, H. B. Schlegel, G. E. Scuseria, M. A. Robb, J. R. Cheeseman, G. Scalmani, V. Barone, G. A. Petersson, H. Nakatsuji, X. Li, M. Caricato, A. Marenich, J. Bloino, B. G. Janesko, R. Gomperts, B. Mennucci, H. P. Hratchian, J. V. Ortiz, A. F. Izmaylov, J. L. Sonnenberg, D. Williams-Young, F. Ding, F. Lipparini, F. Egidi, J. Goings, B. Peng, A. Petrone, T. Henderson, D. Ranasinghe, V. G. Zakrzewski, J. Gao, N. Rega, G.

Zheng, W. Liang, M. Hada, M. Ehara, K. Toyota, R. Fukuda, J. Hasegawa, M. Ishida, T. Nakajima, Y. Honda, O. Kitao, H. Nakai, T. Vreven, K. Throssell, J. A. Montgomery Jr., J. E. Peralta, F. Ogliaro, M. Bearpark, J. J. Heyd, E. Brothers, K. N. Kudin, V. N. Staroverov, T. Keith, R. Kobayashi, J. Normand, K. Raghavachari, A. Rendell, J. C. Burant, S. S. Iyengar, J. Tomasi, M. Cossi, J. M. Millam, M. Klene, C. Adamo, R. Cammi, J. W. Ochterski, R. L. Martin, K. Morokuma, O. Farkas, J. B. Foresman and D. J. Fox, 2016.